Article

Cell Metabolism

Cholesterol Accumulation in Dendritic Cells Links the Inflammasome to Acquired Immunity

Graphical Abstract

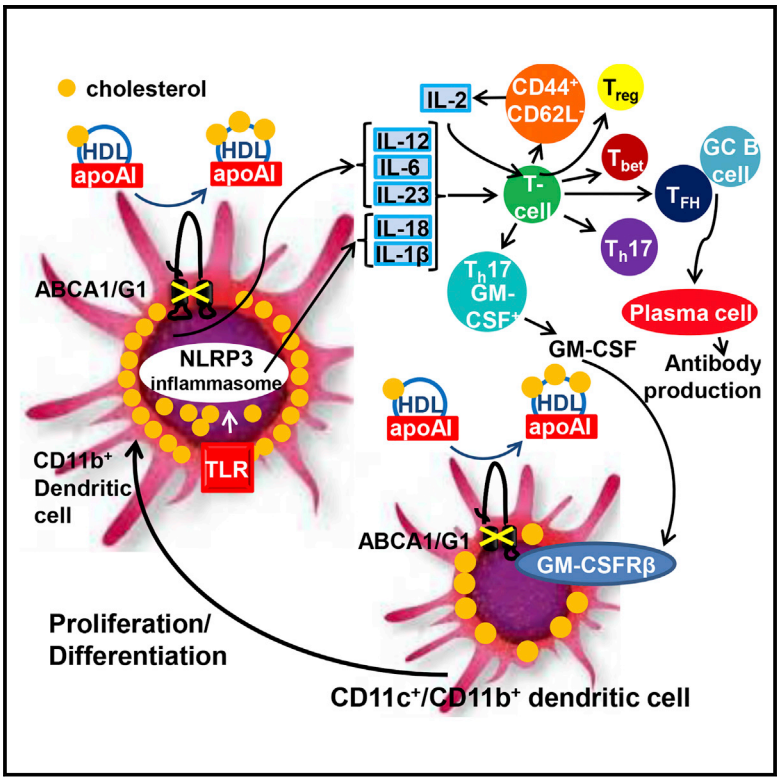

Authors

Marit Westerterp,
Emmanuel L. Gautier, Anjali Ganda, ...,
Vivette D. D'Agati,
Laurent Yvan-Charvet, Alan R. Tall

Correspondence

mw2537@columbia.edu

In Brief

Autoimmune diseases, such as systemic lupus erythematosus (SLE), are associated with reduced plasma high-density lipoproteins (HDL) levels. HDL mediates cholesterol efflux from immune cells via ATP binding cassette transporters A1 and G1 (ABCA1/G1). We show that DC cholesterol accumulation in mice with DC *Abca1/g1* deficiency promotes inflammasome activation and autoimmunity.

Highlights

- Mice with deficiency of *Abca1/g1* in DCs develop autoimmune glomerulonephritis
- Cholesterol-enriched DCs show inflammasome activation and enhanced cytokine secretion
- A GM-CSF driven crosstalk between T_h17 cells and DCs promotes DC proliferation

Westerterp et al., 2017, Cell Metabolism *25*, 1–11
June 6, 2017
http://dx.doi.org/10.1016/j.cmet.2017.04.005

CellPress

Please cite this article in press as: Westerterp et al., Cholesterol Accumulation in Dendritic Cells Links the Inflammasome to Acquired Immunity, Cell Metabolism (2017), http://dx.doi.org/10.1016/j.cmet.2017.04.005

Cell Metabolism
Article

Cholesterol Accumulation in Dendritic Cells Links the Inflammasome to Acquired Immunity

Marit Westerterp,[1,2,6,*] Emmanuel L. Gautier,[3] Anjali Ganda,[1,4] Matthew M. Molusky,[1] Wei Wang,[1] Panagiotis Fotakis,[1] Nan Wang,[1] Gwendalyn J. Randolph,[3] Vivette D. D'Agati,[5] Laurent Yvan-Charvet,[1] and Alan R. Tall[1]
[1]Division of Molecular Medicine, Department of Medicine, Columbia University, 630 West 168 Street, P&S 8-401, New York, NY 10032, USA
[2]Department of Pediatrics, Section Molecular Genetics, University Medical Center Groningen, University of Groningen, 9713 AV Groningen, the Netherlands
[3]Department of Pathology and Immunology, Washington University, St. Louis, MO 63110, USA
[4]Division of Nephrology, Department of Medicine
[5]Department of Pathology
Columbia University, New York, NY 10032, USA
[6]Lead Contact
*Correspondence: mw2537@columbia.edu
http://dx.doi.org/10.1016/j.cmet.2017.04.005

SUMMARY

Autoimmune diseases such as systemic lupus erythematosus (SLE) are associated with increased cardiovascular disease and reduced plasma high-density lipoprotein (HDL) levels. HDL mediates cholesterol efflux from immune cells via the ATP binding cassette transporters A1 and G1 (ABCA1/G1). The significance of impaired cholesterol efflux pathways in autoimmunity is unknown. We observed that *Abca1/g1*-deficient mice develop enlarged lymph nodes (LNs) and glomerulonephritis suggestive of SLE. This lupus-like phenotype was recapitulated in mice with knockouts of *Abca1/g1* in dendritic cells (DCs), but not in macrophages or T cells. DC-*Abca1/g1* deficiency increased LN and splenic CD11b$^+$ DCs, which displayed cholesterol accumulation and inflammasome activation, increased cell surface levels of the granulocyte macrophage-colony stimulating factor receptor, and enhanced inflammatory cytokine secretion. Consequently, DC-*Abca1/g1* deficiency enhanced T cell activation and T_h1 and T_h17 cell polarization. *Nlrp3* inflammasome deficiency diminished the enlarged LNs and enhanced T_h1 cell polarization. These findings identify an essential role of DC cholesterol efflux pathways in maintaining immune tolerance.

INTRODUCTION

Plasma high-density lipoproteins (HDL) concentrations are reduced in patients with systemic lupus erythematosus (SLE) and rheumatoid arthritis (RA) (Norata et al., 2012). These patients have an increased risk of cardiovascular disease (CVD) that cannot be explained by traditional risk factors (Asanuma et al., 2003; Roman et al., 2003; Skeoch and Bruce, 2015). Recent studies have suggested that the capacity of HDL to function as an acceptor for cholesterol efflux is a better predictor of incident CVD than plasma HDL cholesterol concentrations (Khera et al., 2011; Rohatgi et al., 2014). Interestingly, RA disease activity is inversely correlated with the capacity of HDL to function as an acceptor for cellular cholesterol efflux (Ronda et al., 2014). Apolipoprotein A1 (ApoA1) and HDL mediate the efflux of cholesterol from immune cells via the ATP binding cassette transporters A1 and G1 (ABCA1 and ABCG1) (Yvan-Charvet et al., 2007). Whether low HDL and efflux pathways have a causal relationship to autoimmune diseases is unknown.

An almost complete absence of HDL due to deletion of the *apoA1* gene, when combined with genetic and dietary hypercholesterolemia, leads to a partial autoimmune phenotype, characterized by cholesterol engorged, enlarged lymph nodes (LNs), increased plasma autoantibodies to double-stranded DNA (dsDNA), and T cell activation (Wilhelm et al., 2009), suggesting a link between cellular cholesterol accumulation and autoimmunity. Moreover, cholesterol efflux pathways mediated by ABCG1 in T cells have been implicated in T cell proliferative responses and acquired immunity (Armstrong et al., 2010; Bensinger et al., 2008). Autoimmune phenotypes including glomerulonephritis have also been observed in mice with macrophage deficiency of *retinoic X receptor* α (*Rxr*α) or *peroxisome proliferator activated receptor* γ (*Ppar*γ), or whole body deficiency of *liver X receptor* α and β (*Lxr*α and *Lxr*β) (N-Gonzalez et al., 2009; Roszer et al., 2011). Conversely, treatment with an LXR activator inhibited the development of enlarged LNs and glomerulonephritis in a mouse model of SLE, thus ameliorating autoimmunity (N-Gonzalez et al., 2009). The lupus-like phenotypes were attributed to defective macrophage efferocytosis (the uptake of apoptotic bodies), reflecting reduced expression of MerTK, which is an LXR/RXR target mediating efferocytosis (N-Gonzalez et al., 2009; Roszer et al., 2011). The cholesterol efflux promoting ATP binding cassette transporters ABCA1 and ABCG1 are also key transcriptional targets of LXR/RXR (Costet et al., 2000; Kennedy et al., 2005; Wang et al., 2004), suggesting that defective cellular cholesterol efflux could be involved in the autoimmune phenotypes associated with *Lxr* deficiency.

We have developed *Abca1*$^{fl/fl}$*Abcg1*$^{fl/fl}$ mice, which when crossed with appropriate Cre-expressing strains lead to cholesterol accumulation in specific cell types (Westerterp et al., 2012). To investigate a potential role of immune cell cholesterol

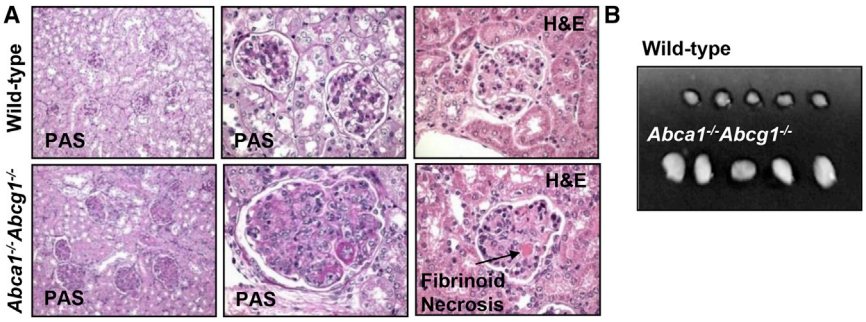

Figure 1. Glomerulonephritis and Enlarged Lymph Nodes in 40-Week-Old *Abca1*$^{-/-}$ *Abcg1*$^{-/-}$ Mice on Chow Diet

Lymph nodes (LNs) and kidneys were collected. Kidneys were embedded in paraffin, sectioned, and stained with H&E and periodic acid-Schiff (PAS).

(A) Glomerulonephritis in *Abca1*$^{-/-}$*Abcg1*$^{-/-}$ and wild-type littermate mice. Fibrinoid necrosis is indicated. Representative pictures of n = 5 mice.

(B) Enlarged LNs in *Abca1*$^{-/-}$*Abcg1*$^{-/-}$ mice compared with wild-type controls. n = 5; representative pictures of three independent experiments.

accumulation in autoimmunity, we first assessed autoimmune phenotypes in mice with *Abca1/g1* deficiency. This revealed enlarged LNs and glomerulonephritis, suggestive of an autoimmune phenotype. However, autoimmune activation was not due to deficiency of transporters in macrophages or T cells, but rather in dendritic cells (DCs). DC-*Abca1/g1* deficiency enlarged the CD11b^{+} DC population, reflecting increased cell surface expression of the common β subunit of the GM-CSF/IL-3 receptor and enhanced proliferation. *Abca1/g1*-deficient CD11b^{+} DCs displayed inflammasome activation and enhanced secretion of inflammatory cytokines, leading to expansion of T and B cell subsets in the spleen and LNs. Deficiency of the *NOD-like receptor family pyrin domain containing 3* (*Nlrp3*) inflammasome partly reversed the enlarged LNs in DC-*Abca1/g1* deficiency, as well as the increase in interleukin-1β (IL-1β) secretion and T_h1 expansion, indicating that this pathway contributes to aspects of the autoimmune phenotype in DC-*Abca1/g1* deficiency.

RESULTS

Abca1$^{-/-}$*Abcg1*$^{-/-}$ Mice and Mice with DC *Abca1/g1* Deficiency Develop an Autoimmune Phenotype

To assess a potential role of cellular cholesterol efflux pathways in acquired immune responses, we characterized mice with general deficiency of *Abca1/g1* for autoimmune phenotypes. At 40 weeks of age, chow-fed *Abca1*$^{-/-}$*Abcg1*$^{-/-}$ mice showed dramatic glomerulonephritis, with enlarged glomeruli, mesangial expansion, diffuse and global endocapillary proliferation, and obliterated capillary lumina. Higher-power images showed infiltrating mononuclear and polymorphonuclear leukocytes in the glomeruli as well as fibrinoid necrosis (Figure 1A). *Abca1*$^{-/-}$*Abcg1*$^{-/-}$ mice also showed enlarged LNs (Figure 1B), consistent with autoimmunity.

To determine which immune cell types might be responsible for these findings, we prepared mice with knockout of both transporters in macrophages, T cells, or DCs by crossing *Abca1*$^{fl/fl}$*Abcg1*$^{fl/fl}$ mice with *LysmCre*, *LckCre*, or *CD11cCre* mice, respectively. These mice are referred to as MAC-ABC^{DKO}, T-ABC^{DKO}, or DC-ABC^{DKO} mice, respectively, with the caveat that *LysmCre* and *CD11cCre* are also partially deleted in monocytes and neutrophils, and *CD11cCre* also in a subset of macrophages (Stranges et al., 2007; Westerterp et al., 2013). In each case, these mice were compared with floxed controls, all in the C57BL6/J background. *Abca1* and *Abcg1* mRNA expression was reduced by >90% in DCs from DC-ABC^{DKO} mice, by >80% in CD4^{+} T cells from T-ABC^{DKO} mice (Figures S1A–S1C), and by >90% in macrophages from MAC-ABC^{DKO} mice (Westerterp et al., 2013). Surprisingly, after 40 weeks of chow diet feeding, kidneys from DC-ABC^{DKO} mice showed evidence of autoimmune glomerulonephritis (Figure 2A), while kidneys from MAC-ABC^{DKO} or T-ABC^{DKO} mice did not show significant pathology (Figures 2B and 2C). Ten out of ten kidneys from DC-ABC^{DKO} mice showed evidence of autoimmune glomerulonephritis, indicating the consistency of this phenotype. Because of a gender bias in autoimmune glomerulonephritis (Kim et al., 2011), we only included female mice in these studies. Further characterization of the glomeruli of DC-ABC^{DKO} mice showed increased staining for various immunoglobulin classes (IgG, IgM, IgA) and complement components (C3 and C1) in the mesangium and peripheral glomerular capillary walls, compared with glomeruli from controls (Figure 2D). The "full house" positive staining for all these five immune reactants closely resembles that seen in active human lupus nephritis (Weening et al., 2004). The increased deposits of IgG, IgM, and IgA in glomeruli of DC-ABC^{DKO} mice were associated with increased plasma autoantibodies to IgG + IgM + IgA dsDNA, which was not observed in MAC-ABC^{DKO} or T-ABC^{DKO} mice (Figure 2E). In addition, DC-ABC^{DKO} mice, but not MAC-ABC^{DKO} or T-ABC^{DKO} mice, exhibited enlarged LNs (Figure 2F), and a temporal increase in plasma IgM and IgG (Figures S1D and S1E). At 20 weeks of age, DC-ABC^{DKO} mice demonstrated only mild mesangial expansion, indicating that the phenotype develops with age, similar to other mouse models developing spontaneous lupus glomerulonephritis (Kim et al., 2011; N-Gonzalez et al., 2009), and paralleling the temporal increase in plasma IgM and IgG (Figures S1D and S1E). DC-ABC^{DKO} mice also had compromised renal function, reflected by increased plasma levels of blood urea nitrogen, creatinine, and uric acid (Figures S1F–S1H). These characteristics all resemble an SLE phenotype. Increased plasma dsDNA antibodies combined with characteristic nephritis is a sufficient criterion for diagnosis of SLE in humans (Petri et al., 2012). Our findings suggest a major role for ABCA1 and ABCG1 expression in DCs in maintaining immune tolerance and preventing autoimmune glomerulonephritis.

Abca1/g1 Deficiency Enhances Cholesterol Accumulation in DCs

We evaluated lipid accumulation in *Abca1/g1*-deficient DCs. DC-*Abca1/g1* deficiency increased BODIPY staining in splenic CD11b^{+} DCs (Figures S1I and S1J), and LNs from DC-ABC^{DKO} mice showed marked enlargement and oil red O staining,

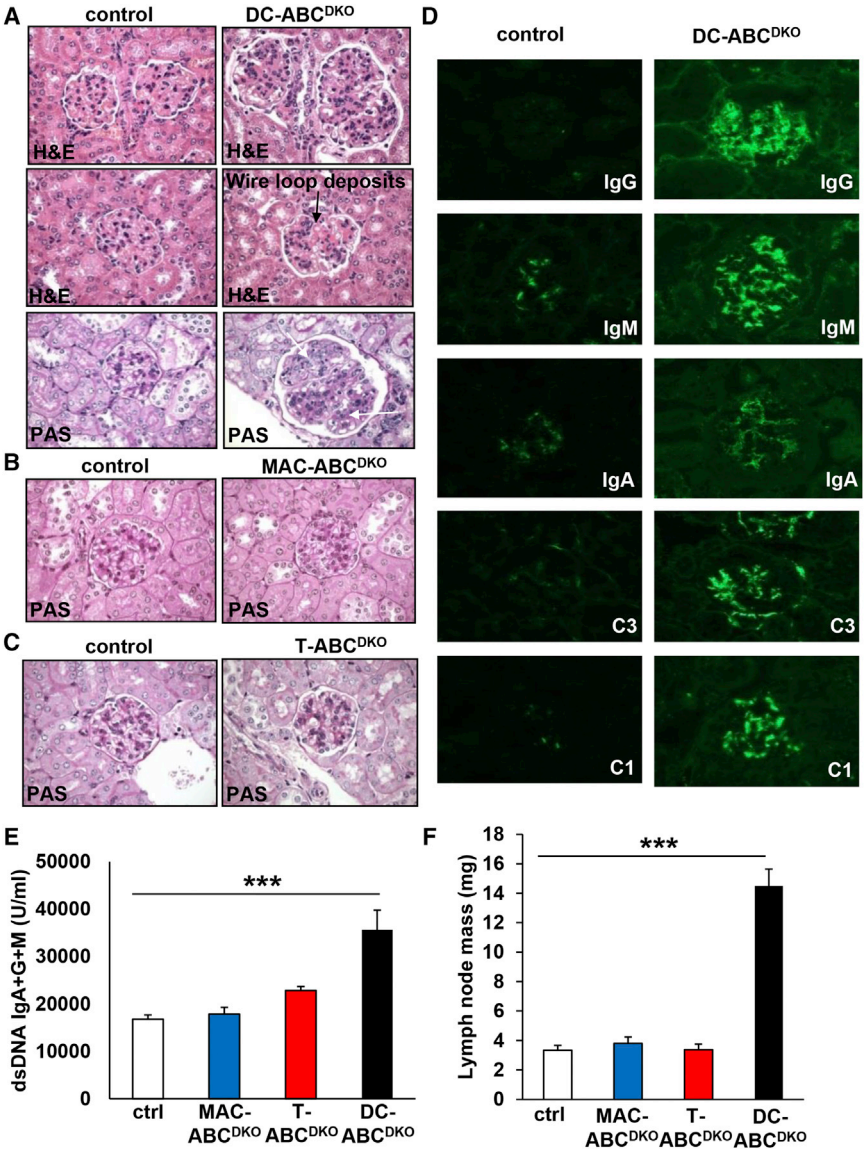

Figure 2. Lupus Glomerulonephritis and Characteristics of an Autoimmune Phenotype in Mice with DC but Not Macrophage or T Cell *Abca1/g1* Deficiency

Mice were fed chow diet for 40 weeks and kidneys, plasma, and LNs were collected. Kidneys were embedded in paraffin, sectioned and stained with H&E and PAS or frozen in OCT, sectioned, and stained as indicated.

(A) Glomerulonephritis in DC-ABC^{DKO} mice. Wire loop deposits (middle panel), infiltrating leukocytes (upper arrow, lower panel) and mesangial hypercellularity (lower arrow, lower panel) are indicated.

(B and C) No glomerulonephritis phenotype in MAC-ABC^{DKO} (B) and T-ABC^{DKO} (C) mice.

(D) Immunoglobulin (IgG, IgM, IgA) and complement components 1 and 3 (C1 and C3) deposits are increased in glomeruli of DC-ABC^{DKO} mice. (A) are representative pictures of n = 10 mice; (B–D) are representative pictures of n = 5 mice.

(E) Increased plasma levels of autoantibodies to dsDNA in DC-ABC^{DKO}, but not MAC-ABC^{DKO} or T-ABC^{DKO} mice. n = 6–10. ***$p < 0.001$ by one-way ANOVA with Bonferroni post-test.

(F) Increased LN mass in DC-ABC^{DKO}, but not MAC-ABC^{DKO} or T-ABC^{DKO} mice. n = 4–8. ***$p < 0.001$ by one-way ANOVA with Bonferroni post-test. Data in (E–F) are presented as mean ± SEM. See also Figure S1.

suggesting neutral lipid accumulation in DCs, i.e., DC "foam cells" (Figure S1K). DC-ABC^{DKO} LN DCs isolated using CD11c^{+} beads and bone marrow-derived DCs also showed evidence of unesterified cholesterol accumulation, as deduced from enzymatic assays or increased filipin staining (Figures S1L–S1N). Possibly as a result of these findings, plasma total cholesterol levels were decreased in DC-*Abca1/g1*-deficient mice (Figure S1O).

DC-*Abca1/g1* Deficiency Increases T Cell Activation

We next determined potential mechanisms responsible for development of autoimmunity in DC-ABC^{DKO} mice. Blood CD4^{+} and CD8^{+} T cells from DC-ABC^{DKO} mice showed increased activation as reflected by a temporal increase in the percentage of CD44^{hi}CD62L^{lo} CD4^{+} and CD8^{+} T cells (Figures 3A–3D), accompanied by increased staining for CXCR3 (Figures 3E and 3F). DC-ABC^{DKO} mice also showed increased CD4^{+} and CD8^{+} T cell activation in LNs (Figure 3G) and spleen (Figure 3H).

The percentage of CD4^{+} and CD8^{+} T cells in DC-ABC^{DKO} mice was similar to controls in blood, and T cell numbers were similar in spleen, but increased in LNs (Figures S2A–S2D). While T cells from control mice did not show proliferation, we observed a low level of proliferation in LN T cells from DC-ABC^{DKO} mice, possibly accounting for the increase in LN size (Figures S2E and S2F). Likely, mainly the CD44^{hi}CD62L^{lo} T cells show enhanced proliferation, as has been described (Tough et al., 1999). Splenic and LN-regulatory T cells (T_{regs}) were also increased (Figures S2G and S2H), probably related to an increase in IL-2 mRNA levels (Figure S2I) in CD44^{hi}CD62L^{lo} CD4^{+} T cells (Boyman and Sprent, 2012).

Expression profiling in DCs (Gautier et al., 2012) shows that all types of DCs have relatively high expression of *Abcg1* with mostly lower expression of *Abca1* (Figure S3A). However, ABCA1 and ABCG1 display overlapping functions and show mutual compensation (Yvan-Charvet et al., 2007), and we found that deficiency of both transporters was required for T cell activation (Figures S3B and S3C), consistent with the previous finding that deletion of ABCA1 or ABCG1 alone did not lead to autoimmune glomerulonephritis (N-Gonzalez et al., 2009).

DC-*Abca1/g1* Deficiency Does Not Affect Antigen Presentation

DCs present antigen to T cells, which requires the interaction of the MHCII complex on DCs with the T cell receptor on T cells, as

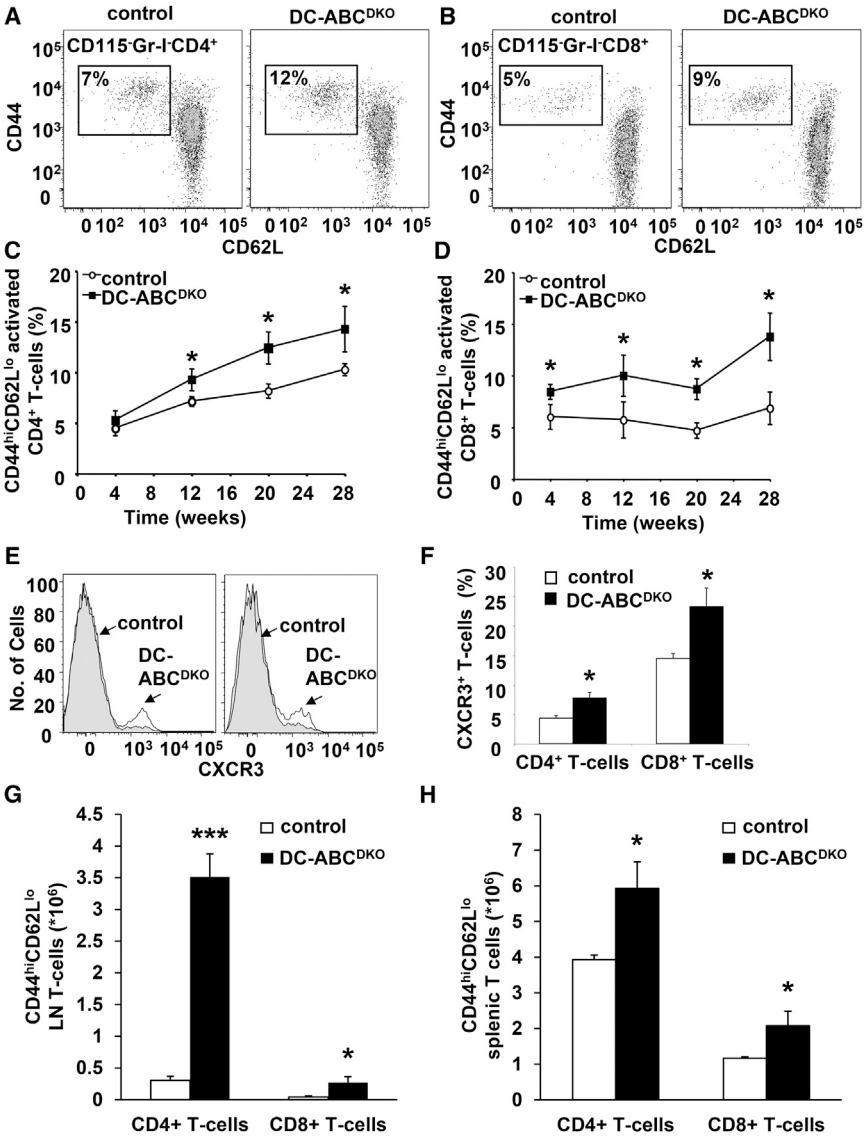

Figure 3. DC-ABC^{DKO} Mice Show Increased T Cell Activation

Blood, LNs, and spleen were collected; LNs and spleen digested using collagenase, and stained with the indicated antibodies and analyzed by flow cytometry.

(A and B) Representative dot plot of activated CD44$^+$CD62L$^-$ CD4$^+$ (A) and CD8$^+$ (B) T cells in blood.

(C and D) Time course of increased CD44$^+$CD62L$^-$ CD4$^+$ (C) and CD8$^+$ (D) T cell activation in blood of DC-ABC^{DKO} mice. n = 8.

(E and F) Increased CXCR3 on CD4$^+$ and CD8$^+$ T cells in blood. (E) Representative plot. (F) CXCR3$^+$ CD4$^+$ and CD8$^+$ T cells. n = 8. Mice were killed after 30 weeks of chow diet.

(G) Increased CD44$^+$CD62L$^-$ CD4$^+$ and CD8$^+$ T cell activation in inguinal LNs of DC-ABC^{DKO} mice. n = 5.

(H) Increased CD44$^+$CD62L$^-$ CD4$^+$ and CD8$^+$ T cell activation in the spleen of DC-ABC^{DKO} mice. n = 7.

***p < 0.001 and *p < 0.05 by t test. Data in (C–D and F–H) are presented as mean ± SEM. See also Figures S2 and S3.

well as co-stimulatory signals such as those mediated by CD80/86 (Freeman et al., 1993). DC-*Abca1/g1* deficiency increased CD11b$^+$, but not CD8a$^+$ DCs (Figures 4A–4C), and did not affect DC surface levels of MHCII (Figures 4D and 4E), while moderately increasing DC surface levels of CD80/86, mainly on CD11b$^+$ DCs (Figures S4A and S4B), and not affecting DC surface levels of PDL-1 on CD11b$^+$ DCs (Figure S4C). We then investigated whether the CD11b$^+$ DCs from DC-ABC^{DKO} mice displayed enhanced antigen presentation. We first immunized DC-ABC^{DKO} mice and their controls with ovalbumin (ova)-peptide and then performed an adoptive transplantation with CD90.1$^+$CD4$^+$ OT-II T cells that specifically recognize ova-MHCII complexes. To monitor proliferation, CD90.1$^+$OT-II CD4$^+$ T cells were labeled with carboxyfluorescein succinimidyl ester (CFSE). We observed similar dilution of the CFSE label in CD90.1$^+$CD4$^+$ T cells in DC-ABC^{DKO} mice and their controls, in both LNs and spleen, indicating no difference in antigen presentation (Figures 4F and 4G). We found that the CD90.1$^+$ marker was essential in distinguishing CFSE-diluted CD4$^+$OT-II cells from the enlarged resident T cell population in DC-ABC^{DKO} mice (results not shown), thus allowing for proper interpretation of the antigen presentation experiments. In vivo, several types of antigen-presenting cells are present, and therefore we also investigated whether DC-*Abca1/g1* deficiency affected antigen presentation in GM-CSF-differentiated bone marrow-derived CD11b$^+$ DCs, with or without lipopolysaccharide treatment (mature and immature DCs, respectively). We incubated these DCs with ova-peptide in the presence of CFSE-labeled CD4$^+$OT-II T cells and found a similar CFSE dilution of T cells incubated with DC-ABC^{DKO} compared with control DCs, both for immature and mature DCs (Figures S4D and S4E), indicating that DC-*Abca1/g1* deficiency also does not affect antigen presentation in vitro. Hence, the increased T cell activation in DC-ABC^{DKO} mice cannot be explained by enhanced antigen presentation. These results are in line with previous observations showing that hypercholesterolemia in *Ldlr*$^{-/-}$ or *Apoe*$^{-/-}$ mice or cholesterol loading of DCs with modified LDL did not affect antigen presentation (Packard et al., 2008).

DC-*Abca1/g1* Deficiency Activates the Inflammasome in CD11b$^+$ DCs

We next explored a potential role of inflammatory pathways in the lupus-like phenotype of DC *Abca1/g1* deficiency. *Abca1/g1* CD11b$^+$ DCs show increased cytokine expression in response to Toll-like receptor (TLR) 3/4 ligands (Westerterp et al., 2012). This may have contributed to T cell activation and proliferation

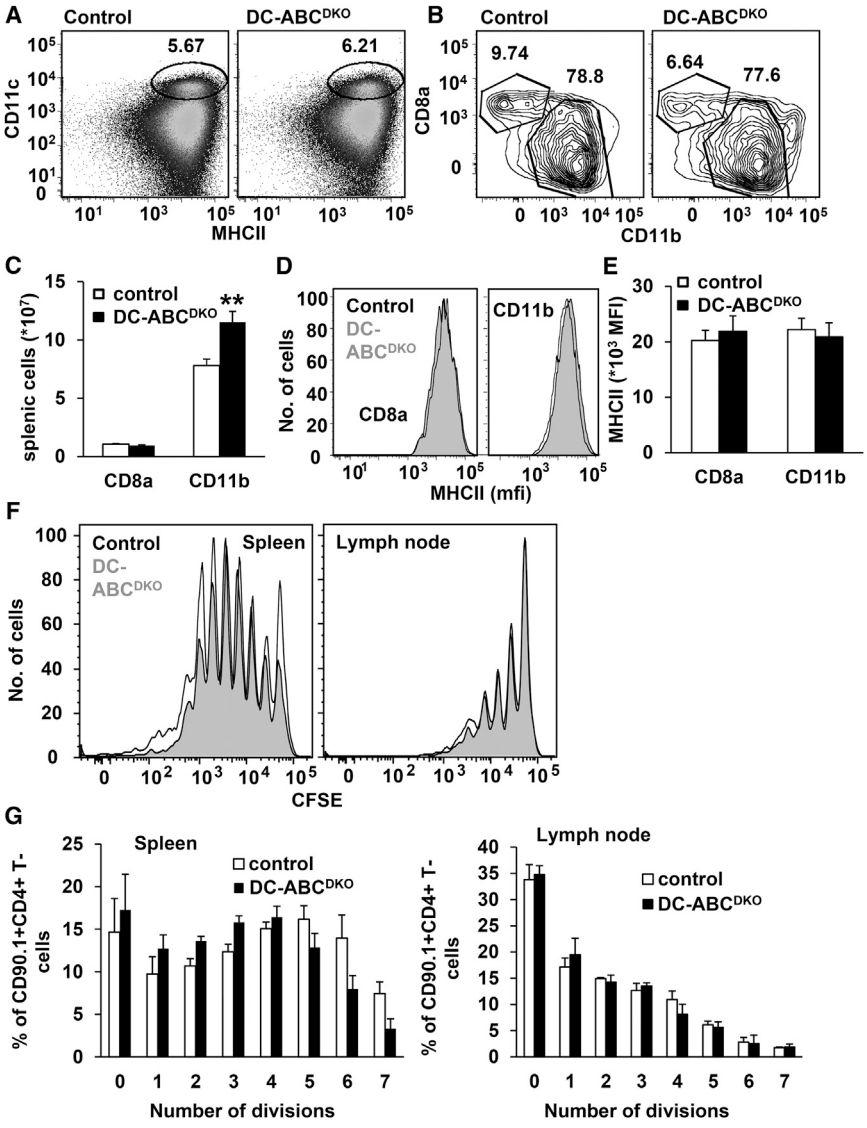

Figure 4. DC *Abca1/g1* Deficiency Does Not Affect Antigen Presentation

Control and DC-ABC^{DKO} mice were 20 weeks old. Spleens were isolated, stained with the indicated antibodies, and analyzed by flow cytometry.

(A and B) Gating strategy of splenic CD11c$^+$ MHCII$^+$CD8a$^+$ and CD11c$^+$MHCII$^+$CD11b$^+$ DCs.

(C) Total splenic CD8a$^+$ and CD11b$^+$ DCs. n = 10.

(D and E) Expression of MHCII on CD8a$^+$ and CD11b$^+$ DCs. n = 6.

(F and G) Antigen presentation. Mice were immunized with ova-peptide. At 24 hr after injection, CD4$^+$ OT-II cells from CD90.1 mice were isolated and labeled with CFSE. A total of 2 × 10^6 cells was injected per mouse and, 72 hr after injection, CFSE dilution in CD90.1$^+$CD4$^+$ T cells was assessed in spleen and inguinal LNs. Representative CFSE dilutions are shown (F) and quantified (G). n = 4.

Data in (C, E, and G) are presented as mean ± SEM. **p < 0.01, by t test. See also Figure S4.

(Tough et al., 1999); however, deficiency of *Trif* or *Myd88* did not reverse T cell activation (Figures S4F–S4G) or the enlarged LN size in DC-ABC^{DKO} mice (results not shown), possibly because of mutual compensation. TLR activation together with cholesterol accumulation activates the NLRP3 inflammasome in immune cells (Sheedy et al., 2013), mediating the secretion of IL-1β and IL-18. The inflammasome is required for IL-18 production, and deficiency of its central enzyme, caspase-1, inhibits lupus glomerulonephritis in mice (Kahlenberg et al., 2014). We found that DC-*Abca1/g1* deficiency enhanced intracellular pro-IL-1β levels in splenic CD11c$^+$CD11b$^+$MHCII$^+$ cells (Figures 5A and 5B), as well as *pro-IL-1β* and *Nlrp3* mRNA (Figures 5C and 5D), indicative of inflammasome priming and likely a consequence of TLR activation (Westerterp et al., 2012). To examine whether DC-*Abca1/g1* deficiency activated the inflammasome, we used beads to isolate CD11b$^+$ cells, >50% of which show expression of CD11c and MHCII (not shown), and measured caspase-1 cleavage, a hallmark of inflammasome activation. We observed that DC-*Abca1/g1* deficiency enhanced caspase-1 cleavage in splenic CD11b$^+$ DCs, and also in LN CD11b$^+$ DCs (Figures 5E–5H). MAC-*Abca1/g1* deficiency did not affect caspase-1 cleavage in LN CD11b$^+$ DCs (Figures 5G and 5H), indicating that the inflammasome activation in LNs was specific for DCs. DC-*Abca1/g1* deficiency also increased IL-18 plasma levels (Figure 5I), further substantiating inflammasome activation in DC-ABC^{DKO} mice. DC-*Abca1/g1* deficiency also increased secretion of IL-1β and IL-18 from splenic CD11b$^+$ cells (Figures 5J and 5K). This was reversed by treatment with reconstituted HDL (rHDL) (Figures 5J and 5K), which can promote cholesterol efflux via passive diffusion, confirming that inflammasome activation depends on cholesterol accumulation in *Abca1/g1*-deficient DCs. In addition, DC-*Abca1/g1* deficiency increased splenic T$_{bet}$$^+$CD4$^+$ T cells (Figures 5L and S5), suggesting skewing of T cells toward T$_h$1 cells, consistent with increased DC IL-18 secretion (Ghayur et al., 1997). Thus, cholesterol accumulation in ABC^{DKO} DCs leads to inflammasome activation, increased secretion of IL-1β and IL-18, and skewing of T cells toward a T$_h$1 phenotype. Interestingly, IL-18 levels are markedly elevated in human SLE, and inflammasome activation contributes to lupus glomerulonephritis in mice (Kahlenberg and Kaplan, 2014; Kahlenberg et al., 2014; Tucci et al., 2008), suggesting a role for inflammasome activation in the autoimmune phenotype of DC-ABC^{DKO} mice.

Deficiency of the NLRP3 Inflammasome Partly Reverses the Autoimmune Phenotype

To assess a contribution of the inflammasome to autoimmune phenotypes, we generated DC-ABC^{DKO} mice with *Nlrp3* deficiency. This partly reversed the increase in LN size compared with DC-ABC^{DKO}*Nlrp3*$^{+/-}$ littermate controls (Figures 6A and

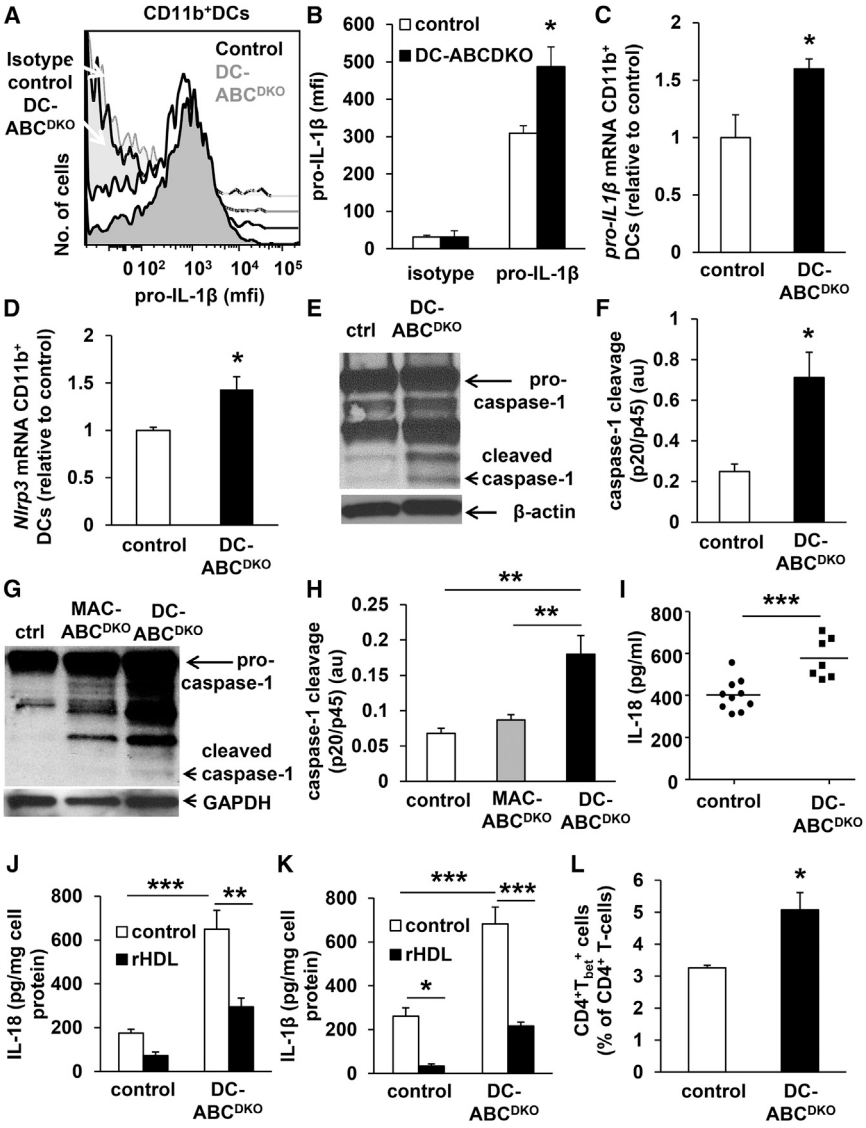

Figure 5. DC *Abca1/g1* Deficiency Activates the Inflammasome and Increases T_h1 Cells

Mice used in all experiments were 20 weeks old unless indicated otherwise.

(A–D) DC-*Abca1/g1* deficiency enhances pro-IL-1β protein (A–B), mRNA levels (C), and *Nlrp3* mRNA levels (D) in splenic $CD11c^+MHCII^+CD11b^+$ cells, indicative of inflammasome priming. FACS plot (A) and quantification (B) are shown. n = 4.

(E–H) From mice of the indicated genotypes, $CD11b^+$ cells were isolated from spleen (E and F) or LNs (G and H) using CD11b-positive beads. Cells were lysed, and caspase-1 cleavage was assessed using western blot. Representative images (E and G) are shown and caspase-1 cleavage was calculated as the ratio of cleaved caspase-1 (p20) to pro-caspase-1 (p45) (F and H). n = 4.

(I) IL-18 plasma levels were assessed in 40 week old DC-ABC^{DKO} and control mice using ELISA. Each data point indicates a single mouse. n = 7–10.

(J and K) $CD11b^+$ cells were isolated from the spleens of control and DC-ABC^{DKO} mice using CD11b-positive beads, and incubated with or without rHDL (o/n). The medium was collected and the secretion of IL-1β (J) and IL-18 (K) was assessed using ELISA, and corrected for cell protein. n = 4.

(L) Splenic cell homogenates were stained with an antibody to CD4, fixed and permeabilized, and stained for T_{bet} (L) or its isotype control. For quantification, values were corrected for their respective isotype controls. n = 5.

Data in (B–D, F, H, and J–L) are presented as mean ± SEM. (B–D, F, I, and L), *p < 0.05, **p < 0.01, ***p < 0.001, by t test. (H, J, and K), *p < 0.05, **p < 0.01, ***p < 0.001, by one-way ANOVA with Bonferroni post-test. See also Figure S5.

6B), indicating an important contribution of the NLRP3 inflammasome to aspects of the autoimmune phenotype of DC-ABC^{DKO} mice. Consistent with the role of the inflammasome in regulating IL-1β secretion, *Nlrp3* deficiency decreased IL-1β secretion from DC-ABC^{DKO} $CD11b^+$ cells (Figure 6C). *Nlrp3* deficiency also decreased splenic $T_{bet}^+CD4^+$ T cells in DC-ABC^{DKO} mice (Figures 6D and 6E), likely due to a decrease in local IL-18 secretion from splenic DC-ABC^{DKO}*Nlrp3*$^{-/-}$ DCs. These results thus suggest that the *Nlrp3* inflammasome contributes to aspects of the autoimmune phenotype in DC-ABC^{DKO} mice.

Increased GM-CSF Receptor-β and Cytokine Secretion from $CD11b^+$ ABC^{DKO} DCs

Since *Nlrp3* deficiency only partly reversed the autoimmune phenotype of DC-ABC^{DKO} mice, we sought to define additional mechanisms regulating inflammation. We had observed that the $CD11b^+$ DC population was expanded in DC-ABC^{DKO} mice (Figure 4C). *Abca1/g1* deficiency in hematopoietic stem and progenitor cells increases the cell surface expression of the common β subunit of the IL-3/GM-CSF receptor, increasing the proliferation of these cells (Yvan-Charvet et al., 2010). We found that DC-*Abca1/g1* deficiency increased the cell surface but not mRNA levels of the common β subunit of the IL-3/GM-CSF receptor on splenic $CD11b^+$ DCs (Figures 7A and 7B and S6A–S6C) together with $CD11b^+$ DC proliferation (Figures 7C and 7D), likely accounting for the increased number of $CD11b^+$ DCs (Figure 4C), and suggesting enhanced GM-CSF-induced differentiation of $CD11c^+$ into $CD11b^+$ DCs.

DC secretion of IL-23, IL-12, and IL-6 contributes to autoimmune phenotypes. Previous studies have suggested that GM-CSF induces the secretion of these cytokines by DCs (Codarri et al., 2011; El-Behi et al., 2011; Sonderegger et al., 2008), linking GM-CSF signaling with autoimmunity. We found that DC-*Abca1/g1* deficiency in splenic $CD11c^+CD11b^+MHCII^+$ cells markedly enhanced intracellular expression of IL-6 and p40, the subunit of both IL-23 and IL-12, as well as *Il-23p19* mRNA expression (Figures S6D–S6H), likely due to enhanced TLR activation in these cells (Westerterp et al., 2012). The secretion of these cytokines from splenic $CD11b^+$ cells was also increased, with reversal by rHDL treatment (Figures 7E–7G). We also found

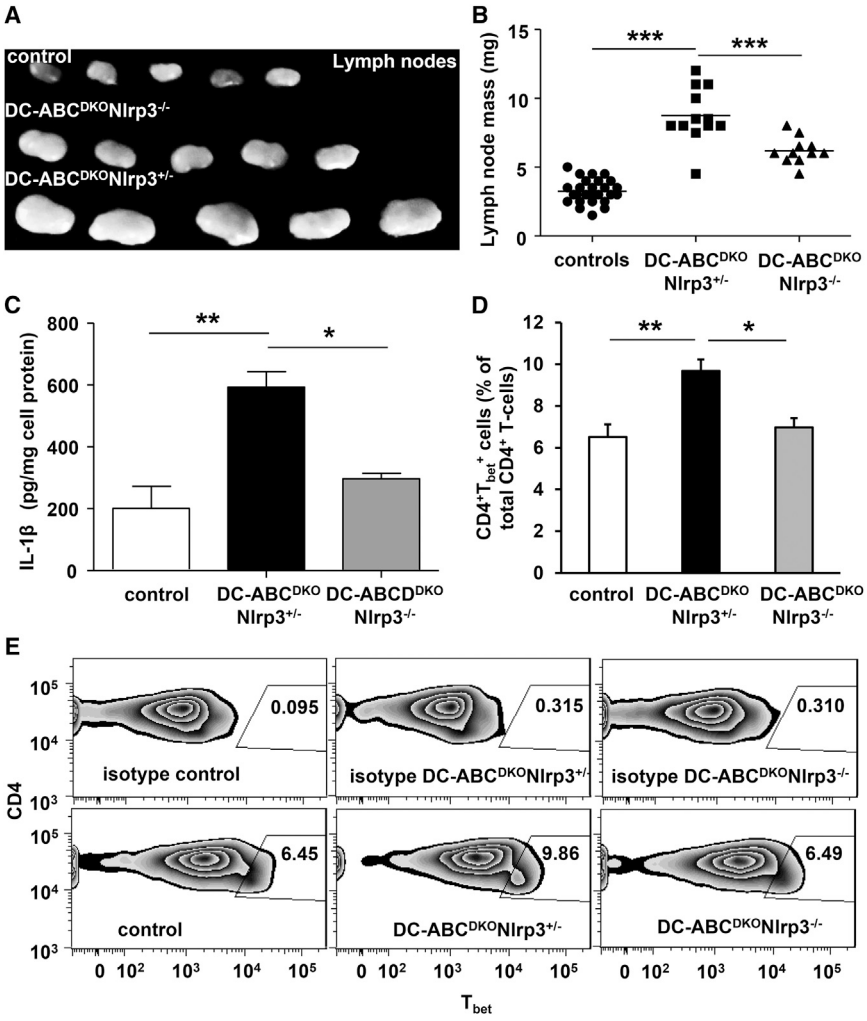

Figure 6. *Nlrp3* Deficiency Reverses Part of the Phenotype of DC-ABC^{DKO} Mice

Abca1$^{fl/fl}$Abcg1$^{fl/fl}$Nlrp3$^{+/-}$, *Abca1$^{fl/fl}$Abcg1$^{fl/fl}$Nlrp3$^{-/-}$* (referred to as controls), DC-ABC^{DKO} Nlrp3$^{+/-}$, and DC-ABC^{DKO}Nlrp3$^{-/-}$ mice were 10 weeks old.

(A and B) LNs were isolated. Representative pictures are shown (A) and LNs were weighed (B). n = 11–25. Splenic CD11b$^+$ cells were isolated and IL-1β secretion (o/n) was assessed (C). n = 5–10. Splenic cell homogenates were stained with an antibodies to CD4, fixed and permeabilized, and stained for T$_{bet}$ or its isotype control. CD4$^+$T$_{bet}^+$ T cells were assessed and values were corrected for their respective isotype controls (D and E). n = 5–8. Data in (B, C, and E) are presented as mean ± SEM. *p < 0.05, **p < 0.01, ***p < 0.001, by one-way ANOVA with Bonferroni post-test.

that DC-*Abca1/g1* deficiency enhanced GM-CSF-induced secretion of IL-23, IL-12, and IL-6 in splenic CD11c$^+$ DCs (Figures S6I–S6K). This may reflect GM-CSF-induced differentiation of CD11c$^+$ into inflammatory CD11b$^+$ DCs (Campbell et al., 2011) in vivo, as DC-ABC^{DKO} CD11b$^+$ DCs were increased in numbers (Figure 4C) and showed increased interleukin secretion without a requirement for added GM-CSF ex vivo (Figures 7E–7G). These studies thus link the increased expression of the common β subunit of the GM-CSF receptor on *Abca1/g1*-deficient DCs with proliferation of CD11b$^+$ DCs that show inflammasome activation and enhanced secretion of a variety of inflammatory cytokines.

DC-*Abca1/G1* Deficiency Increases T and B Cell Subsets

We then investigated whether T and B cell subsets that are known to be responsive to these DC interleukins were expanded. IL-1β, IL-6, and IL-23 induce T$_h$17 differentiation (Acosta-Rodriguez et al., 2007). We observed that splenic CD4$^+$IL17A$^+$ T cells were dramatically increased over time in DC-ABC^{DKO} mice compared with controls, reflecting T$_h$17 expansion (Figures 7H–7J). Similar results were found in LNs (not shown). Even though MAC-ABC^{DKO} mice also showed an increase in plasma IL-23 and IL-17 in previous studies, these mice did not develop lupus glomerulonephritis in the current study (Figure 2B), likely reflecting modest increases in plasma IL-23 and IL-17 compared with DC-ABC^{DKO} mice (Westerterp et al., 2012). Consistent with T$_h$17 cell expansion and T cell activation (Campbell et al., 2011; Codarri et al., 2011; El-Behi et al., 2011), we also found that DC-*Abca1/g1* deficiency enhanced splenic GM-CSF$^+$CD4$^+$ and GM-CSF$^+$ CD8$^+$ T cells (Figures 7K and 7L); 80% of GM-CSF$^+$CD4$^+$ T cells were positive for IL17A, suggesting they are a subset of T$_h$17 cells (Figures S7A–S7B). These T cells, by secreting GM-CSF, could sustain the differentiation of CD11c$^+$ into CD11b$^+$ DCs that secrete T cell activating cytokines, suggestive of a previously identified positive feedback loop in which GM-CSF sustains interleukin production by DCs (El-Behi et al., 2011). To test the hypothesis that these effects on T cells were caused by *Abca1/g1* deficiency in DCs, we co-incubated splenic DCs from DC-ABC^{DKO} mice and controls with naive T cells. After 5 days, DC-*Abca1/g1* deficiency increased differentiation of naive T cells into T$_h$17 or GM-CSF$^+$ T cells (Figures S7C–S7F), indicating the effect on T cells was secondary to the DC *Abca1/g1* deficiency.

We next investigated whether DC-*Abca1/g1* deficiency affected T follicular helper (T$_{FH}$) and germinal center (GC) B cells, since a previous study suggested that IL-6 secretion by DCs led to expansion of these cells and caused SLE (Kim et al., 2011). Splenic T$_{FH}$ and GC B cells were increased in DC-*Abca1/g1*-deficient mice compared with their controls (Figures S7G–S7J), and we also observed an increase in short-lived plasma cells that are present in GCs (Figures 7K and 7L). Further supporting B cell proliferation and differentiation, and contributing to T$_{FH}$ accumulation (Coquery et al., 2015), plasma levels of B cell-activating factor (BAFF) were increased in DC-*Abca1/g1*-deficient mice compared with their controls (Figure S7M). In sum, these findings show that deficiency of cholesterol efflux pathways in

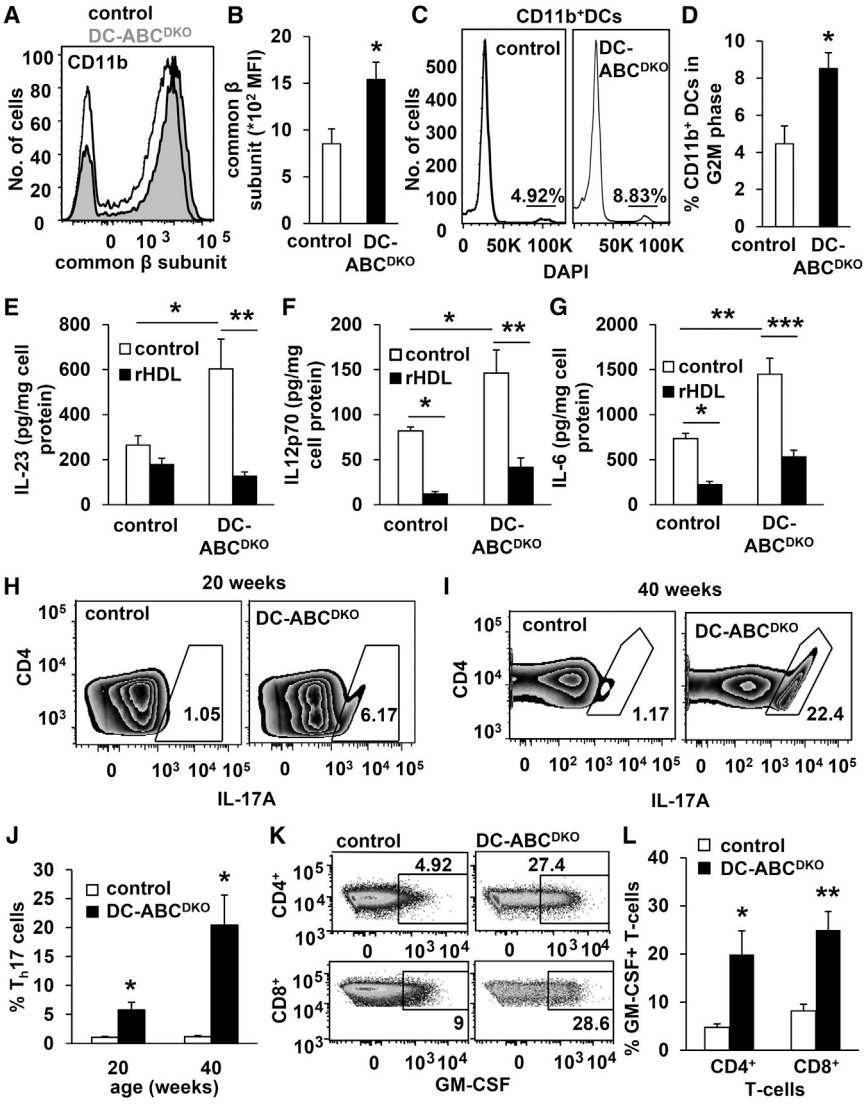

Figure 7. DC *Abca1/g1* Deficiency Increases Surface Expression of the Common β Subunit of the GM-CSF Receptor, DC Proliferation, Secretion of Interleukins with Reversal by rHDL, and T and B Cell Subsets

Mice used in all experiments were 20 weeks old unless indicated otherwise. Spleens were isolated (A–D), stained for DC markers in combination with the indicated antibodies, and analyzed by flow cytometry.

(A and B) DC-*Abca1/g1* deficiency increases the common β subunit of the GM-CSF receptor on splenic CD11b$^+$ DCs. n = 6.

(C and D) DC-*Abca1/g1* deficiency increased the percentage of CD11b$^+$ DCs in the G2M phase, calculated using the Watson model. n = 4.

(E–G) CD11b$^+$ cells were isolated from the spleens of control and DC-ABC^{DKO} mice using CD11b-positive beads, and incubated with or without rHDL (o/n). The medium was collected and the secretion of IL23p19 (E), IL12p70 (F), and IL-6 (G) was assessed using ELISA, and corrected for cell protein. n = 4.

(H–L) Splenic cell homogenates were stained with antibodies to CD4 (H-L), TCRβ, and CD8 (K–L), fixed and permeabilized, stained for IL17A (H–J), or GM-CSF (K–L), and T_h17 cells (defined as CD4$^+$IL17A$^+$) (H–J) and GM-CSF$^+$ T cells (K–L) were measured using flow cytometry. n = 5.

Data in (B, D–G, J, and L) are presented as mean ± SEM. (B, J, and L) *p < 0.05, **p < 0.01, ***p < 0.001, by t test. (D–G) *p < 0.05, **p < 0.01, ***p < 0.001, by one-way ANOVA with Bonferroni post-test. See also Figures S6 and S7.

DCs promotes inflammasome activation and inflammatory cytokine secretion that leads to a dramatic expansion of T_h17 cells, and increases in T_h1 T cells, T_{FH} cells, GC B cells, plasma cells, and in BAFF plasma levels, changes which have previously been linked to the development of SLE (Kim et al., 2011; Kyttaris et al., 2010; Pisitkun et al., 2012).

DISCUSSION

Our findings indicate that cholesterol efflux pathways in DCs have a key role in preventing cholesterol accumulation and maintaining immune tolerance. Mice with DC *Abca1/g1* deficiency in the non-perturbed homeostatic state developed a marked autoimmune phenotype. In contrast, deletion of these transporters in macrophages or T cells did not lead to autoimmunity, indicating a mechanism distinct from previous observations involving reduced MerTK in *Lxr*-, *Pparγ*-, or *Rxr*-deficient macrophages or *Abcg1* deficiency in T cells (Bensinger et al., 2008; N-Gonzalez et al., 2009; Roszer et al., 2011). DC *Abca1/g1* deficiency activated the inflammasome, increased cell surface expression of the common β subunit for the GM-CSF receptor, CD11b$^+$ DC proliferation, and secretion of a variety of cytokines from CD11b$^+$ DCs, leading to expansion of activated T cells, T_h17 cells, GM-CSF$^+$ T cells, T_h1 cells, T_{FH} cells, GC B cells, and plasma cells, all changes that have been implicated in the pathogenesis of SLE. Thus, cholesterol accumulation in DCs promotes autoimmunity, predominantly through activation of inflammatory signaling pathways.

Deficiency of the *Nlrp3* inflammasome diminished the increases in LN size, DC IL-1β secretion, and T_{bet}^+ T cells in DC-ABC^{DKO} mice, indicating an essential contribution of the inflammasome to key aspects of the autoimmune phenotype in DC-ABC^{DKO} mice. The NLRP3 inflammasome is activated in several autoimmune diseases including RA and SLE. Factors that induce lupus glomerulonephritis, such as neutrophil extracellular traps, self dsDNA, and complement C3a activate the NLRP3 inflammasome in human monocytes and macrophages (Asgari et al., 2013; Kahlenberg et al., 2013; Mathews et al., 2014; Shin et al., 2013). Polymorphisms in *NLRP3* or *IL-18* (Kahlenberg and Kaplan, 2014) have been associated with SLE risk, and plasma IL-18 levels with disease activity (Kahlenberg et al., 2014; Tucci et al., 2008). In mouse models, inhibition of the P_2X_7 receptor, which is essential for ATP-mediated NLRP3

inflammasome activation, *caspase-1* deficiency, and *Il-18 receptor* deficiency protect against lupus glomerulonephritis (Kahlenberg et al., 2014; Kinoshita et al., 2004; Zhao et al., 2013). Our study provides direct evidence for a role for the NLRP3 inflammasome in regulating aspects of the autoimmune phenotype in DC-ABC^{DKO} mice, and for the first time relates inflammasome activation in DCs to cholesterol accumulation. Inflammasome priming is likely increased by enhanced TLR signaling via cholesterol-enriched membrane lipid rafts as shown previously in *Abca1/g1* deficient cells (Westerterp et al., 2012; Yvan-Charvet et al., 2008), similar to macrophages (Sheedy et al., 2013). However, we did not observe inflammasome activation in LN CD11b$^+$ cells from MAC-ABC^{DKO} mice, probably reflecting a paucity of inflammatory CD11b$^+$ cells in the LNs.

In addition to the inflammasome-mediated secretion of IL-1β and IL-18, cholesterol accumulation in splenic *Abca1/g1*-deficient CD11b$^+$ DCs enhanced the secretion of IL-6, IL-23p19, and IL-12p70, which have been shown to promote autoimmunity (Sonderegger et al., 2008). Lupus patients also show an increase in T_h17 cells and deficiency of the *Il-23 receptor* or *Il-17* impairs the development of lupus glomerulonephritis in mice (Kyttaris et al., 2010; Pisitkun et al., 2012). It is thus likely that cholesterol-induced secretion of IL-1β, IL-6, and IL-23p19 by DCs, which induce T_h17 expansion (Acosta-Rodriguez et al., 2007), contributes to lupus glomerulonephritis in DC-*Abca1/g1* deficiency. Since inflammasome activation is involved in IL-1β secretion it may also link to the observed increase in GM-CSF$^+$ T_h17 cells. Multiple mechanisms of inflammatory cytokine production likely explain why the reversal of autoimmunity by *Nlrp3* deficiency was only partial. Complexity and heterogeneity may also explain the failure of several interventions targeting specific cytokines in human SLE (Narain and Furie, 2016).

Our data suggest that cholesterol accumulation in DCs leads to both increased GM-CSF receptor levels and increased cytokine secretion, and thus engages a positive feedback loop wherein GM-CSF-secreting T_h17 cells promote differentiation of CD11c$^+$ into CD11b$^+$ DCs expressing high levels of the GM-CSF receptor, enhancing proliferation, and further cytokine production (Graphical Abstract), as suggested in earlier studies of autoimmune diseases (El-Behi et al., 2011; Lin et al., 2016). GM-CSF enhances cytokine secretion by CD11c$^+$ DCs (Sonderegger et al., 2008), presumably because of its crucial role in differentiating CD11c$^+$ into CD11b$^+$ DCs (Campbell et al., 2011). Our findings suggest that, in addition to previous autoimmune models such as EAE, this positive feedback loop plays a role in lupus.

Although our findings were made using a specific model in which cholesterol efflux pathways are deleted in DCs, similar principles may be involved in other settings in which hypercholesterolemia is associated with autoimmunity (Wilhelm et al., 2009). *Apoe*$^{-/-}$ mice show increased plasma autoantibodies to dsDNA and accelerated glomerulonephritis when crossed with *gld* mice, or simply in response to feeding a high-cholesterol diet. This was attributed to decreased apoptotic cell clearance (Aprahamian et al., 2004; Wang et al., 2014). *Apoa1* and *Apoe* deficiency decrease plasma HDL levels in mice, potentially leading to DC inflammasome activation and enhanced cytokine secretion that activate T cells, as suggested by our study. *Apoe*$^{-/-}$ mice also show increased splenic T_h17 cells (Westerterp et al., 2012), which could have contributed to the lupus phenotype. A recent study showed that mice with whole-body deficiency of *Apoe* and *Lxrβ* mice develop an autoimmune phenotype, associated with lipid accumulation in CD11c$^+$ cells. Autoimmunity was attributed to enhanced antigen presentation as shown in *Lxrαβ*$^{-/-}$ mice (Ito et al., 2016). Similar to our study, CD11c$^+$MHCII$^+$ cells were expanded in *Apoe*$^{-/-}$*CD11cCreLxrβ*$^{fl/fl}$ mice and BAFF levels were increased. In contrast, we did not observe any difference in antigen presentation with either in vivo or in vitro assays (Figures 4F, 4G, S4D, and S4E). The reason for this apparent discrepancy is unclear. Previous studies have shown that hypercholesterolemia in *Apoe*$^{-/-}$ mice and cholesterol accumulation in DCs induced by loading with modified lipoproteins does not affect antigen presentation (Packard et al., 2008).

In general, inflammatory stimuli, such as interferon-γ (Panousis and Zuckerman, 2000) or TLR3/4 activation (Castrillo et al., 2003), suppress cholesterol efflux pathways. Our studies suggest that, in autoimmune disorders such as SLE or RA, inflammatory suppression of HDL levels and of cholesterol efflux pathways and cholesterol accumulation in DCs amplifies autoimmune responses. In this setting, treatments employing LXR activators to upregulate ABCA1/G1, or cholesterol-poor reconstituted HDL that mediate diffusional, non-transporter-dependent cholesterol efflux (Cuchel et al., 2010) and were shown to be anti-inflammatory in CD11b$^+$ DCs in the present study, may have therapeutic benefit. The role of statins in ameliorating autoimmune phenotypes remains unclear (Khattri and Zandman-Goddard, 2013), but also warrants systematic investigation.

STAR★METHODS

Detailed methods are provided in the online version of this paper and include the following:

- KEY RESOURCES TABLE
- CONTACT FOR REAGENT AND RESOURCE SHARING
- EXPERIMENTAL MODEL DETAILS
  - Animals
- METHOD DETAILS
  - Kidney and LN Analysis, ELISAs
  - Differentiation of Dendritic Cells *In Vitro*
  - Filipin Staining
  - Flow Cytometry
  - Microarray
  - Antigen Presentation *In Vivo*
  - Antigen Presentation *In Vitro*
  - Primary DC Isolation and Analysis, DC-T-Cell Co-incubation Experiments
- QUANTIFICATION AND STATISTICAL ANALYSIS
- DATA AND SOFTWARE AVAILABILITY

SUPPLEMENTAL INFORMATION

Supplemental Information includes seven figures and can be found with this article online at http://dx.doi.org/10.1016/j.cmet.2017.04.005.

AUTHOR CONTRIBUTIONS

M.W., E.L.G., A.G., M.M.M., W.W., N.W., V.D.D., and L.Y.-C. designed and performed the experiments. G.J.R. was involved in the experimental design

of the project. M.W. and A.R.T. wrote the manuscript. All authors reviewed the manuscript. A.R.T. supervised, designed, and reviewed the entire project.

ACKNOWLEDGMENTS

This work has been supported by NIH grants HL107653 (to A.R.T.), T32HL007343 (to M.M.M.), the Netherlands Organization of Scientific Research VIDI-grant 917.15.350 (to M.W.), a UMCG Rosalind Franklin Fellowship (to M.W.), and an American Heart Association SDG2160053 grant (to L.Y.-C.). Flow cytometry experiments were performed in the CCTI Flow Cytometry Core, supported in part by the Office of the Director, NIH under awards S10RR027050. The content is solely the responsibility of the authors and does not necessarily represent the official views of the NIH. A.R.T. reports being a consultant to Amgen and CSL.

Received: February 19, 2016
Revised: November 4, 2016
Accepted: April 6, 2017
Published: May 4, 2017

REFERENCES

Acosta-Rodriguez, E.V., Napolitani, G., Lanzavecchia, A., and Sallusto, F. (2007). Interleukins 1beta and 6 but not transforming growth factor-beta are essential for the differentiation of interleukin 17-producing human T helper cells. Nat. Immunol. *8*, 942–949.

Aprahamian, T., Rifkin, I., Bonegio, R., Hugel, B., Freyssinet, J.M., Sato, K., Castellot, J.J., Jr., and Walsh, K. (2004). Impaired clearance of apoptotic cells promotes synergy between atherogenesis and autoimmune disease. J. Exp. Med. *199*, 1121–1131.

Armstrong, A.J., Gebre, A.K., Parks, J.S., and Hedrick, C.C. (2010). ATP-binding cassette transporter G1 negatively regulates thymocyte and peripheral lymphocyte proliferation. J. Immunol. *184*, 173–183.

Asanuma, Y., Oeser, A., Shintani, A.K., Turner, E., Olsen, N., Fazio, S., Linton, M.F., Raggi, P., and Stein, C.M. (2003). Premature coronary-artery atherosclerosis in systemic lupus erythematosus. N. Engl. J. Med. *349*, 2407–2415.

Asgari, E., Le Friec, G., Yamamoto, H., Perucha, E., Sacks, S.S., Kohl, J., Cook, H.T., and Kemper, C. (2013). C3a modulates IL-1beta secretion in human monocytes by regulating ATP efflux and subsequent NLRP3 inflammasome activation. Blood *122*, 3473–3481.

Bensinger, S.J., Bradley, M.N., Joseph, S.B., Zelcer, N., Janssen, E.M., Hausner, M.A., Shih, R., Parks, J.S., Edwards, P.A., Jamieson, B.D., and Tontonoz, P. (2008). LXR signaling couples sterol metabolism to proliferation in the acquired immune response. Cell *134*, 97–111.

Boyman, O., and Sprent, J. (2012). The role of interleukin-2 during homeostasis and activation of the immune system. Nat. Rev. Immunol. *12*, 180–190.

Campbell, I.K., van Nieuwenhuijze, A., Segura, E., O'Donnell, K., Coghill, E., Hommel, M., Gerondakis, S., Villadangos, J.A., and Wicks, I.P. (2011). Differentiation of inflammatory dendritic cells is mediated by NF-kappaB1-dependent GM-CSF production in CD4 T cells. J. Immunol. *186*, 5468–5477.

Castrillo, A., Joseph, S.B., Vaidya, S.A., Haberland, M., Fogelman, A.M., Cheng, G., and Tontonoz, P. (2003). Crosstalk between LXR and toll-like receptor signaling mediates bacterial and viral antagonism of cholesterol metabolism. Mol. Cell *12*, 805–816.

Codarri, L., Gyulveszi, G., Tosevski, V., Hesske, L., Fontana, A., Magnenat, L., Suter, T., and Becher, B. (2011). RORgammat drives production of the cytokine GM-CSF in helper T cells, which is essential for the effector phase of autoimmune neuroinflammation. Nat. Immunol. *12*, 560–567.

Coquery, C.M., Loo, W.M., Wade, N.S., Bederman, A.G., Tung, K.S., Lewis, J.E., Hess, H., and Erickson, L.D. (2015). BAFF regulates follicular helper t cells and affects their accumulation and interferon-gamma production in autoimmunity. Arthr Rheumatol. *67*, 773–784.

Costet, P., Luo, Y., Wang, N., and Tall, A.R. (2000). Sterol-dependent transactivation of the ABC1 promoter by the liver X receptor/retinoid X receptor. J. Biol. Chem. *275*, 28240–28245.

Cuchel, M., Lund-Katz, S., de la Llera-Moya, M., Millar, J.S., Chang, D., Fuki, I., Rothblat, G.H., Phillips, M.C., and Rader, D.J. (2010). Pathways by which reconstituted high-density lipoprotein mobilizes free cholesterol from whole body and from macrophages. Arterioscler. Thromb. Vasc. Biol. *30*, 526–532.

El-Behi, M., Ciric, B., Dai, H., Yan, Y., Cullimore, M., Safavi, F., Zhang, G.X., Dittel, B.N., and Rostami, A. (2011). The encephalitogenicity of T(H)17 cells is dependent on IL-1- and IL-23-induced production of the cytokine GM-CSF. Nat. Immunol. *12*, 568–575.

Freeman, G.J., Borriello, F., Hodes, R.J., Reiser, H., Hathcock, K.S., Laszlo, G., McKnight, A.J., Kim, J., Du, L., Lombard, D.B., et al. (1993). Uncovering of functional alternative CTLA-4 counter-receptor in B7-deficient mice. Science *262*, 907–909.

Gautier, E.L., Shay, T., Miller, J., Greter, M., Jakubzick, C., Ivanov, S., Helft, J., Chow, A., Elpek, K.G., Gordonov, S., et al. (2012). Gene-expression profiles and transcriptional regulatory pathways that underlie the identity and diversity of mouse tissue macrophages. Nat. Immunol. *13*, 1118–1128.

Ghayur, T., Banerjee, S., Hugunin, M., Butler, D., Herzog, L., Carter, A., Quintal, L., Sekut, L., Talanian, R., Paskind, M., et al. (1997). Caspase-1 processes IFN-gamma-inducing factor and regulates LPS-induced IFN-gamma production. Nature *386*, 619–623.

Ito, A., Hong, C., Oka, K., Salazar, J.V., Diehl, C., Witztum, J.L., Diaz, M., Castrillo, A., Bensinger, S.J., Chan, L., and Tontonoz, P. (2016). Cholesterol accumulation in CD11c+ immune cells is a causal and targetable factor in autoimmune disease. Immunity *45*, 1311–1326.

Kahlenberg, J.M., Carmona-Rivera, C., Smith, C.K., and Kaplan, M.J. (2013). Neutrophil extracellular trap-associated protein activation of the NLRP3 inflammasome is enhanced in lupus macrophages. J. Immunol. *190*, 1217–1226.

Kahlenberg, J.M., and Kaplan, M.J. (2014). The inflammasome and lupus: another innate immune mechanism contributing to disease pathogenesis? Curr. Opin. Rheumatol. *26*, 475–481.

Kahlenberg, J.M., Yalavarthi, S., Zhao, W., Hodgin, J.B., Reed, T.J., Tsuji, N.M., and Kaplan, M.J. (2014). An essential role of caspase 1 in the induction of murine lupus and its associated vascular damage. Arthr Rheumatol. *66*, 152–162.

Kennedy, M.A., Barrera, G.C., Nakamura, K., Baldan, A., Tarr, P., Fishbein, M.C., Frank, J., Francone, O.L., and Edwards, P.A. (2005). ABCG1 has a critical role in mediating cholesterol efflux to HDL and preventing cellular lipid accumulation. Cell Metab. *1*, 121–131.

Khattri, S., and Zandman-Goddard, G. (2013). Statins and autoimmunity. Immunol. Res. *56*, 348–357.

Khera, A.V., Cuchel, M., de la Llera-Moya, M., Rodrigues, A., Burke, M.F., Jafri, K., French, B.C., Phillips, J.A., Mucksavage, M.L., Wilensky, R.L., et al. (2011). Cholesterol efflux capacity, high-density lipoprotein function, and atherosclerosis. N. Engl. J. Med. *364*, 127–135.

Kim, S.J., Zou, Y.R., Goldstein, J., Reizis, B., and Diamond, B. (2011). Tolerogenic function of Blimp-1 in dendritic cells. J. Exp. Med. *208*, 2193–2199.

Kinoshita, K., Yamagata, T., Nozaki, Y., Sugiyama, M., Ikoma, S., Funauchi, M., and Kanamaru, A. (2004). Blockade of IL-18 receptor signaling delays the onset of autoimmune disease in MRL-Faslpr mice. J. Immunol. *173*, 5312–5318.

Kyttaris, V.C., Zhang, Z., Kuchroo, V.K., Oukka, M., and Tsokos, G.C. (2010). Cutting edge: IL-23 receptor deficiency prevents the development of lupus nephritis in C57BL/6-lpr/lpr mice. J. Immunol. *184*, 4605–4609.

Lin, C.C., Bradstreet, T.R., Schwarzkopf, E.A., Jarjour, N.N., Chou, C., Archambault, A.S., Sim, J., Zinselmeyer, B.H., Carrero, J.A., Wu, G.F., et al. (2016). IL-1-induced Bhlhe40 identifies pathogenic T helper cells in a model of autoimmune neuroinflammation. J. Exp. Med. *213*, 251–271.

Mathews, R.J., Robinson, J.I., Battellino, M., Wong, C., Taylor, J.C., Biologics in Rheumatoid Arthritis Genetics and Genomics Study Syndicate (BRAGGSS), Eyre, S., Churchman, S.M., Wilson, A.G., Isaacs, J.D., et al. (2014). Evidence of NLRP3-inflammasome activation in rheumatoid arthritis (RA); genetic variants within the NLRP3-inflammasome complex in relation to susceptibility to RA and response to anti-TNF treatment. Ann. Rheum. Dis. *73*, 1202–1210.

N-Gonzalez, A., Bensinger, S.J., Hong, C., Beceiro, S., Bradley, M.N., Zelcer, N., Deniz, J., Ramirez, C., Diaz, M., Gallardo, G., et al. (2009). Apoptotic cells promote their own clearance and immune tolerance through activation of the nuclear receptor LXR. Immunity *31*, 245–258.

Narain, S., and Furie, R. (2016). Update on clinical trials in systemic lupus erythematosus. Curr. Opin. Rheumatol. *28*, 477–487.

Norata, G.D., Pirillo, A., Ammirati, E., and Catapano, A.L. (2012). Emerging role of high density lipoproteins as a player in the immune system. Atherosclerosis *220*, 11–21.

Packard, R.R., Maganto-Garcia, E., Gotsman, I., Tabas, I., Libby, P., and Lichtman, A.H. (2008). CD11c(+) dendritic cells maintain antigen processing, presentation capabilities, and CD4(+) T-cell priming efficacy under hypercholesterolemic conditions associated with atherosclerosis. Circ. Res. *103*, 965–973.

Panousis, C.G., and Zuckerman, S.H. (2000). Interferon-gamma induces downregulation of Tangier disease gene (ATP-binding-cassette transporter 1) in macrophage-derived foam cells. Arterioscler. Thromb. Vasc. Biol. *20*, 1565–1571.

Petri, M., Orbai, A.M., Alarcon, G.S., Gordon, C., Merrill, J.T., Fortin, P.R., Bruce, I.N., Isenberg, D., Wallace, D.J., Nived, O., et al. (2012). Derivation and validation of the Systemic Lupus International Collaborating Clinics classification criteria for systemic lupus erythematosus. Arthr Rheumatol. *64*, 2677–2686.

Pisitkun, P., Ha, H.L., Wang, H., Claudio, E., Tivy, C.C., Zhou, H., Mayadas, T.N., Illei, G.G., and Siebenlist, U. (2012). Interleukin-17 cytokines are critical in development of fatal lupus glomerulonephritis. Immunity *37*, 1104–1115.

Rohatgi, A., Khera, A., Berry, J.D., Givens, E.G., Ayers, C.R., Wedin, K.E., Neeland, I.J., Yuhanna, I.S., Rader, D.R., de Lemos, J.A., and Shaul, P.W. (2014). HDL cholesterol efflux capacity and incident cardiovascular events. N. Engl. J. Med. *371*, 2383–2393.

Roman, M.J., Shanker, B.A., Davis, A., Lockshin, M.D., Sammaritano, L., Simantov, R., Crow, M.K., Schwartz, J.E., Paget, S.A., Devereux, R.B., and Salmon, J.E. (2003). Prevalence and correlates of accelerated atherosclerosis in systemic lupus erythematosus. N. Engl. J. Med. *349*, 2399–2406.

Ronda, N., Favari, E., Borghi, M.O., Ingegnoli, F., Gerosa, M., Chighizola, C., Zimetti, F., Adorni, M.P., Bernini, F., and Meroni, P.L. (2014). Impaired serum cholesterol efflux capacity in rheumatoid arthritis and systemic lupus erythematosus. Ann. Rheum. Dis. *73*, 609–615.

Roszer, T., Menendez-Gutierrez, M.P., Lefterova, M.I., Alameda, D., Nunez, V., Lazar, M.A., Fischer, T., and Ricote, M. (2011). Autoimmune kidney disease and impaired engulfment of apoptotic cells in mice with macrophage peroxisome proliferator-activated receptor gamma or retinoid X receptor alpha deficiency. J. Immunol. *186*, 621–631.

Sheedy, F.J., Grebe, A., Rayner, K.J., Kalantari, P., Ramkhelawon, B., Carpenter, S.B., Becker, C.E., Ediriweera, H.N., Mullick, A.E., Golenbock, D.T., et al. (2013). CD36 coordinates NLRP3 inflammasome activation by facilitating intracellular nucleation of soluble ligands into particulate ligands in sterile inflammation. Nat. Immunol. *14*, 812–820.

Shin, M.S., Kang, Y., Lee, N., Wahl, E.R., Kim, S.H., Kang, K.S., Lazova, R., and Kang, I. (2013). Self double-stranded (ds)DNA induces IL-1beta production from human monocytes by activating NLRP3 inflammasome in the presence of anti-dsDNA antibodies. J. Immunol. *190*, 1407–1415.

Skeoch, S., and Bruce, I.N. (2015). Atherosclerosis in rheumatoid arthritis: is it all about inflammation? Nat. Rev. Rheumatol. *11*, 390–400.

Sonderegger, I., Iezzi, G., Maier, R., Schmitz, N., Kurrer, M., and Kopf, M. (2008). GM-CSF mediates autoimmunity by enhancing IL-6-dependent Th17 cell development and survival. J. Exp. Med. *205*, 2281–2294.

Stranges, P.B., Watson, J., Cooper, C.J., Choisy-Rossi, C.M., Stonebraker, A.C., Beighton, R.A., Hartig, H., Sundberg, J.P., Servick, S., Kaufmann, G., et al. (2007). Elimination of antigen-presenting cells and autoreactive T cells by Fas contributes to prevention of autoimmunity. Immunity *26*, 629–641.

Tough, D.F., Sun, S., Zhang, X., and Sprent, J. (1999). Stimulation of naive and memory T cells by cytokines. Immunol. Rev. *170*, 39–47.

Tucci, M., Quatraro, C., Lombardi, L., Pellegrino, C., Dammacco, F., and Silvestris, F. (2008). Glomerular accumulation of plasmacytoid dendritic cells in active lupus nephritis: role of interleukin-18. Arthr Rheumatol. *58*, 251–262.

Wang, N., Lan, D., Chen, W., Matsuura, F., and Tall, A.R. (2004). ATP-binding cassette transporters G1 and G4 mediate cellular cholesterol efflux to high-density lipoproteins. Proc. Natl. Acad. Sci. USA *101*, 9774–9779.

Wang, Y., Lu, H., Huang, Z., Lin, H., Lei, Z., Chen, X., Tang, M., Gao, F., Dong, M., Li, R., and Lin, L. (2014). Apolipoprotein E-knockout mice on high-fat diet show autoimmune injury on kidney and aorta. Biochem. Biophys. Res. Commun. *450*, 788–793.

Weening, J.J., D'Agati, V.D., Schwartz, M.M., Seshan, S.V., Alpers, C.E., Appel, G.B., Balow, J.E., Bruijn, J.A., Cook, T., Ferrario, F., et al. (2004). The classification of glomerulonephritis in systemic lupus erythematosus revisited. J. Am. Soc. Nephrol. *15*, 241–250.

Westerterp, M., Gourion-Arsiquaud, S., Murphy, A.J., Shih, A., Cremers, S., Levine, R.L., Tall, A.R., and Yvan-Charvet, L. (2012). Regulation of hematopoietic stem and progenitor cell mobilization by cholesterol efflux pathways. Cell Stem Cell *11*, 195–206.

Westerterp, M., Murphy, A.J., Wang, M., Pagler, T.A., Vengrenyuk, Y., Kappus, M.S., Gorman, D.J., Nagareddy, P.R., Zhu, X., Abramowicz, S., et al. (2013). Deficiency of ATP-binding cassette transporters A1 and G1 in macrophages increases inflammation and accelerates atherosclerosis in mice. Circ. Res. *112*, 1456–1465.

Wilhelm, A.J., Zabalawi, M., Grayson, J.M., Weant, A.E., Major, A.S., Owen, J., Bharadwaj, M., Walzem, R., Chan, L., Oka, K., et al. (2009). Apolipoprotein A-I and its role in lymphocyte cholesterol homeostasis and autoimmunity. Arterioscler. Thromb. Vasc. Biol. *29*, 843–849.

Yvan-Charvet, L., Ranalletta, M., Wang, N., Han, S., Terasaka, N., Li, R., Welch, C., and Tall, A.R. (2007). Combined deficiency of ABCA1 and ABCG1 promotes foam cell accumulation and accelerates atherosclerosis in mice. J. Clin. Invest. *117*, 3900–3908.

Yvan-Charvet, L., Welch, C., Pagler, T.A., Ranalletta, M., Lamkanfi, M., Han, S., Ishibashi, M., Li, R., Wang, N., and Tall, A.R. (2008). Increased inflammatory gene expression in ABC transporter-deficient macrophages: free cholesterol accumulation, increased signaling via toll-like receptors, and neutrophil infiltration of atherosclerotic lesions. Circulation *118*, 1837–1847.

Yvan-Charvet, L., Pagler, T., Gautier, E.L., Avagyan, S., Siry, R.L., Han, S., Welch, C.L., Wang, N., Randolph, G.J., Snoeck, H.W., and Tall, A.R. (2010). ATP-binding cassette transporters and HDL suppress hematopoietic stem cell proliferation. Science *328*, 1689–1693.

Zhao, J., Wang, H., Dai, C., Wang, H., Zhang, H., Huang, Y., Wang, S., Gaskin, F., Yang, N., and Fu, S.M. (2013). P2X7 blockade attenuates murine lupus nephritis by inhibiting activation of the NLRP3/ASC/caspase 1 pathway. Arthr Rheumatol. *65*, 3176–3185.

STAR★METHODS

KEY RESOURCES TABLE

REAGENT or RESOURCE	SOURCE	IDENTIFIER
Antibodies		
CD11c-PerCP-Cy5.5	BD Pharmingen	Cat# 560584; RRID: AB_1727422
CD11c-PE-Cy7	BD Pharmingen	Cat# 561022; RRID: AB_2033997
CD138-APC	BD Pharmingen	Cat# 561705; RRID: AB_10896819
CD45-APC-Cy7	BD Pharmingen	Cat# 557659; RRID: AB_396774
common β subunit IL-3/GM-CSFRβ (CD131)-PE	BD Pharmingen	Cat# 559920; RRID: AB_397374
Ly6-C/G-PerCP-Cy5.5	BD Pharmingen	Cat# 561103; RRID: AB_10562568
B220-FITC	Biolegend	Cat# 103225; RRID: AB_10573502
CD19-PE	Biolegend	Cat# 152408; RRID: AB_2629817
CD80-PB	Biolegend	Cat# 104724; RRID: AB_2075999
TCRβ-PB	Biolegend	Cat# 109226; RRID: AB_1027649
CD115-PE	eBioscience	Cat# 12-1152; RRID: AB_465808
CD11b-APC	eBioscience	Cat# 17-0112; RRID: AB_469343
CD11b-PB (eFluor 450)	eBioscience	Cat# 48-0112; RRID: AB_1582237
CD4-APC	eBioscience	Cat# 17-0041; RRID: AB_469320
CD4-PB (eFluor 450)	eBioscience	Cat# 48-0041; RRID: AB_10718983
CD44-PE-Cy7	eBioscience	Cat# 25-0441; RRID: AB_469623
CD62L-APC	eBioscience	Cat# 17-0621; RRID: AB_469410
CD8-FITC	eBioscience	Cat# 9011-0087; RRID: AB_10754061
CD8a-APC-Cy7	eBioscience	Cat# 47-0081; RRID: AB_1272221
CD86-PE	eBioscience	Cat# 12-0862; RRID: AB_465768
CD90.1-PE	eBioscience	Cat# 12-0900; RRID: AB_465773
CD90.2-FITC	eBioscience	Cat# 11-0903; RRID: AB_465156
CXCR3-APC	eBioscience	Cat# 17-1831; RRID: AB_1210791
CXCR5- PerCP-Cy5.5 (eFluor 710)	eBioscience	Cat# 46-7185; RRID: AB_2573837
F480-PE-Cy7	eBioscience	Cat# 25-4801; RRID: AB_469653
GL7-APC (eFluor 660)	eBioscience	Cat# 50-5902; RRID: AB_2574252
GM-CSF-PE	eBioscience	Cat# 12-7331; RRID: AB_466204
MHCII-FITC	eBioscience	Cat# 11-5321; RRID: AB_465232
PD1-FITC	eBioscience	Cat# 11-9985; RRID: AB_465472
PD-L1-PE	eBioscience	Cat# 12-5982; RRID: AB_466089
pro-IL-1β-PE	eBioscience	Cat# 12-7114; RRID: AB_10732630
Isotype control-PE (pro-IL-1β)	eBioscience	Cat# 12-4301; RRID: AB_470046
p40-APC (eFluor 660)	eBioscience	Cat# 50-7123; RRID: AB_11218493
Isotype control-APC (p40)	eBioscience	Cat# 50-4321; RRID: AB_10598503
IL-6-PB (eFluor 450)	eBioscience	Cat# 48-7061; RRID: AB_2574103
Isotype control-PB (IL-6)	eBioscience	Cat# 48-4301; RRID: AB_1271988
IL17A-FITC (Alexa Fluor 488)	eBioscience	Cat# 53-7177; RRID: AB_763579
T_{bet}-PE	eBioscience	Cat# 12-5825; RRID: AB_925762
Isotype control-PE (T_{bet})	eBioscience	Cat# 12-4714; RRID: AB_470059
Caspase-1	eBioscience	Cat# 14-9832; RRID: AB_2016691
Rat secondary (for caspase-1)	Cell Signaling	Cat# 7077; RRID: AB_10694715
Chemicals, Peptides, and Recombinant Proteins		
OVA (323 - 339) (OT-II peptide) *ISQAVHAAHAEINEAGR*	Anaspec	AS-27024
Violet Proliferation Dye (CFSE)	BD Horizon	562158

(*Continued on next page*)

Continued

REAGENT or RESOURCE	SOURCE	IDENTIFIER
Recombinant murine GM-CSF	Peprotech	315-03
Recombinant murine IL-4	Peprotech	214-14
Filipin complex	Sigma Aldrich	F9765
Oil Red O	Sigma Aldrich	O0625
Bodipy 493/503	Thermo Fisher	D3922
Critical Commercial Assays		
Uric acid detection	Roche Diagnostics	03183807190
BUN detection	Roche Diagnostics	04460715190
Creatinine detection	Roche Diagnostics	03263991190
CD11c microbeads, ultrapure, mouse	Miltenyi Biotec	130-108-338
CD11b microbeads, mouse (and human)	Miltenyi Biotec	130-049-601
CD4 (L3T4) microbeads, mouse	Miltenyi Biotec	130-049-201
CD3ε microbeads, mouse	Miltenyi Biotec	130-094-973
Cholesterol E (total cholesterol assay)	Wako Diagnostics	999-02601
Free Cholesterol E (free cholesterol assay)	Wako Diagnostics	993-02501
Mouse IgG ELISA Kit	Alpha Diagnostic International	6320
Mouse IgM ELISA Kit	Alpha Diagnostic International	6380
Mouse anti-dsDNA Ig's (total A+G+M) ELISA kit	Alpha Diagnostic International	5110
Mouse BAFF ELISA kit	R&D Systems	MBLYS0
Mouse IL-1β ELISA kit	R&D Systems	MLB00C
Mouse IL-18 ELISA kit	R&D Systems	7625
Mouse IL-23 ELISA kit	R&D Systems	M2300
Mouse IL-12p70 ELISA kit	R&D Systems	M1270
Mouse IL-6 ELISA kit	R&D Systems	M6000B
Mouse Regulatory T-cell Kit	eBioscience	88-8111
Deposited Data		
Microarray Analysis GSE#15907	Immunological Genome Project http://www.immgen.org Gautier et al., 2012	N/A.
Experimental Models: Organisms/Strains		
mouse: Abca1$^{-/-}$: DBA/1-*Abca1*^{tm1Jdm}/J	The Jackson Laboratory	JAX 003897
mouse: Abcg1$^{-/-}$	Deltagen; Kennedy et al., 2005	N/A.
mouse: Abca1$^{fl/fl}$Abcg1$^{fl/fl}$: B6.Cg-*Abca1*^{tm1Jp} *Abcg1*^{tm1Tall}/J	The Jackson Laboratory	JAX 021067
mouse: LysmCre: B6.129P2-*Lyz2*$^{tm1(cre)Ifo}$/J	The Jackson Laboratory	JAX 004781
mouse: CD11cCre: B6.Cg-Tg(Itgax-cre)1-1Reiz/J	The Jackson Laboratory	JAX 008068
mouse: LckCre: B6.Cg-Tg(Lck-cre)548Jxm/J	The Jackson Laboratory	JAX 003802
mouse: Myd88$^{fl/fl}$: B6.129P2(SJL)-*Myd88*^{tm1Defr}/J	The Jackson Laboratory	JAX 008888
mouse: Trif$^{-/-}$: C57BL/6J-*Ticam1*^{Lps2}/J	The Jackson Laboratory	JAX 005037
mouse: Nlrp3$^{-/-}$: B6.129S6-*Nlrp3*^{tm1Bhk}/J	The Jackson Laboratory	JAX 021302
mouse: OT II: B6.Cg-Tg(TcraTcrb)425Cbn/J	The Jackson Laboratory	JAX 004194
mouse: CD90.1 (Thy 1.1): B6.PL-*Thy1*^{a}/CyJ	The Jackson Laboratory	JAX 000406
Oligonucleotides		
Mouse Abca1fl/fl forward primer 5'-GTGAATGGGCAATTCGCAAACT-3'	This paper	N/A
Mouse Abca1fl/fl reverse primer 5'-AGATCTCCCCTCCTTGACAATGC-3'	This paper	N/A
Mouse Abcg1fl/fl forward primer 5'-TGTTCAGGAGGCCATGATGGT-3'	This paper	N/A

(*Continued on next page*)

Continued

REAGENT or RESOURCE	SOURCE	IDENTIFIER
Mouse Abcg1fl/fl reverse primer 5'-TGGCCAGGCGTTTCCG-3'	This paper	N/A
Mouse Nlrp3 forward primer 5′-ATTACCCGCCCGAGAAAGG-3′	This paper	N/A
Mouse Nlrp3 reverse primer 5′-TCGCAGCAAAGATCCACACAG-3′	This paper	N/A
Mouse pro-IL-1β forward primer 5′-TGTGAATGCCACCTTTTGACA-3′	This paper	N/A
Mouse pro-IL-1β reverse primer 5′-GGTCAAAGGTTTGGAAGCAG-3′	This paper	N/A
Mouse IL-23 forward primer 5'-CGCCAAGGTCTGGCTTTTT-3'	This paper	N/A
Mouse IL-23 reverse primer 5'- CGCTGCCACTGCTGACTAGA-3'	This paper	N/A
Software and Algorithms		
FACS DiVa software	BD Biosciences	https://www.bdbiosciences.com/us/instruments/research/software/flow-cytometry-acquisition/bd-facsdiva-software/m/111112/overview
FlowJo	FlowJo	https://www.flowjo.com/solutions/flowjo
GraphPad Prism version 5.01	GraphPad Software	https://www.graphpad.com/scientific-software/prism/

CONTACT FOR REAGENT AND RESOURCE SHARING

Further information and requests for resources and reagents should be directed to and will be fulfilled by Marit Westerterp (mw2537@columbia.edu or m.westerterp@umcg.nl).

EXPERIMENTAL MODEL DETAILS

Animals

Abca1$^{-/-}$*Abcg1*$^{-/-}$ mice and wild-type littermate controls in the mixed DBA/C57Bl6/J background were generated as described previously (Yvan-Charvet et al., 2007) by crossbreeding *Abcg1*$^{-/-}$ mice (DeltaGen; subsequently backcrossed 10 times into the C57Bl/6J background) with *Abca1*$^{-/-}$ mice in the DBA background (Jackson Laboratories, stock number 003897). All other mice were in the C57Bl6/J background. We have deposited *Abca1*$^{fl/fl}$*Abcg1*$^{fl/fl}$ mice at Jackson Laboratories (stock number 021067). *LysmCreAbca1*$^{fl/fl}$*Abcg1*$^{fl/fl}$, *CD11cCreAbca1*$^{fl/fl}$*Abcg1*$^{fl/fl}$, and *LckCreAbca1*$^{fl/fl}$*Abcg1*$^{fl/fl}$ mice were generated by crossbreeding *Abca1*$^{fl/fl}$*Abcg1*$^{fl/fl}$ mice with *LysmCre*, *CD11cCre*, and *LckCre* mice (Jackson Laboratories, stock numbers 004781, 008068, and 003802, respectively). *CD11cCreAbca1*$^{fl/fl}$*Abcg1*$^{fl/fl}$*Myd88*$^{fl/fl}$, *Abca1*$^{fl/fl}$*Abcg1*$^{fl/fl}$*Myd88*$^{fl/fl}$, *CD11cCreAbca1*$^{fl/fl}$*Abcg1*$^{fl/fl}$*Trif*$^{-/-}$, *Abca1*$^{fl/fl}$*Abcg1*$^{fl/fl}$*Trif*$^{-/-}$, *CD11cCreAbca1*$^{fl/fl}$*Abcg1*$^{fl/fl}$*Nlrp3*$^{-/-}$, and *Abca1*$^{fl/fl}$*Abcg1*$^{fl/fl}$*Nlrp3*$^{-/-}$ mice were generated by cross-breeding *CD11cCreAbca1*$^{fl/fl}$*Abcg1*$^{fl/fl}$ with *Myd88*$^{fl/fl}$, *Trif*$^{-/-}$, or *Nlrp3*$^{-/-}$ mice (Jackson Laboratories, stock numbers 008888, 005037, and 021302, respectively). OT-II mice were from Jackson Laboratories (stock number 004194) and CD90.1 OT-II mice were kindly provided by Dr. Hao Wei Li and Dr. Megan Sykes and were bred at Columbia University by intercrossing CD90.1 (also referred to as Thy1.1) mice (Jackson Laboratories, stock number 000406) with OT-II mice.

For all studies, littermates were used, and mice were housed under SPF conditions in cages (4-5 mice per cage) with micro-isolator tops with a 12 h light cycle (7 am -7 pm) and fed an irradiated chow diet (Purina Mills Diet 5053). Housing temperatures were kept within a range of 71-73°F (21.7-22.8°C). Water and cages were autoclaved. Cages were changed once weekly, and the health status of the mice was monitored using a dirty bedding sentinel program. The mouse genotype did not cause changes in weight (mouse weight between 20-30 g, depending on gender and age), health or immune status. Female littermates (lupus glomerulonephritis studies) or littermates from both sexes were randomly assigned to experimental groups, unless stated otherwise. The age and number of the mice used for the experiments are indicated for each experiment in the figure legends. In general, n=4-10 mice were used per group and experiments were repeated at least once if n=4 mice were used per experiment to confirm the reproducibility of the results. No inclusion or exclusion criteria were used. All protocols were approved by the Institutional Animal Care and Use Committee of Columbia University.

METHOD DETAILS

Kidney and LN Analysis, ELISAs

At 20 or 40 weeks of age, *Abca1*$^{-/-}$*Abcg1*$^{-/-}$ or wild-type female mice were sacrificed. At 40 weeks of age DC-ABC^{DKO}, MAC-ABC^{DKO}, and T-ABC^{DKO}, and their respective littermate control groups were sacrificed (all females). Kidneys were dissected, and one kidney per mouse was fixed in 10% phosphate buffered formalin. Kidneys were then embedded in paraffin, 2 μm sections were made, which were stained with hematoxylin & eosin (H&E) and periodic acid-Schiff (PAS). The other kidney was embedded in OCT, frozen, and 2 μm sections were made, and stained with FITC-conjugated rabbit antibodies to IgG, IgM, IgA, complement C3 or complement C1 (Dako, Carpinteria, CA). These procedures were performed in a blinded fashion, *i.e.* the analysis was done by an independent observer, unaware of the genotypes. n=5-10 mice were used per genotype.

Inguinal lymph nodes (LNs) were isolated concomitantly with the kidneys, and adipose tissue was removed from LNs. LNs were weighed and pictures were taken from *Abca1*$^{-/-}$*Abcg1*$^{-/-}$ and wild-type LNs (and in later experiments also from LNs of DC-ABC^{DKO}Nlrp3$^{+/-}$, DC-ABC^{DKO}Nlrp3$^{-/-}$ mice, and their littermate controls). LNs from DC-ABC^{DKO} mice and their controls were fixed and embedded in OCT compound and immediately frozen on dry ice. Frozen cross-sections were made (5 μm), stained for Oil Red O, and counterstained with haematoxylin. Pictures were taken using an Olympus IX-70 microscope equipped with a mercury 100-W lamp (CHIU Technical Corp.), an Olympus LCPlanF1 ×100 objective, DP Manager Basic imaging software (version 3.1; Olympus), and an Olympus DP71 CCD camera. To assess cholesterol accumulation in LN DCs from DC-ABC^{DKO} mice and their controls, LNs were meshed in PBS on a 40 μm filter, cells were collected and DCs were isolated using CD11c^{+} beads (Miltenyi Biotec, CA). Lipids were extracted using the Folch method, and cholesterol levels analyzed using an enzymatic assay (Wako Diagnostics, USA). n=4-8 mice per genotype were used for each experiment described above, and n=11-25 mice per genotype for experiments in DC-ABC^{DKO}Nlrp3$^{+/-}$, DC-ABC^{DKO}Nlrp3$^{-/-}$ mice, and their littermate controls.

From the same abovementioned DC-ABC^{DKO}, MAC-ABC^{DKO}, T-ABC^{DKO}, and their respective controls, also blood was drawn using heparin coated capillaries and kept on ice. Blood was then centrifuged at 10000 rpm for 10 min at 4°C and serum was collected, and immediately assayed for auto-antibodies to dsDNA (IgA+G+M; Alpha Diagnostic International). For serum from DC-ABC^{DKO} mice, uric acid, BUN, and creatinine were measured using specific detection kits in conjunction with a Cobas C311 analyzer (Roche Diagnostics). In addition to these measurements, in serum from 10, 20, and 40 weeks old control and DC-ABC^{DKO} mice (littermates from both sexes randomly assigned to control and DC-ABC^{DKO} group), BAFF, IgM, and IgG levels were measured using ELISA (IgM and IgG, Alpha Diagnostic International; BAFF, R&D Systems). n=10 mice per genotype were used for these experiments.

Differentiation of Dendritic Cells *In Vitro*

Bone marrow (BM) was isolated from DC-ABC^{DKO} and control mice. Red blood cells (RBCs) were lysed (BD Pharm Lyse, BD Bioscience), and BM was incubated in DMEM containing 10% FBS and 1% pen strep supplemented with 10 ng/ml GM-CSF and 10 ng/ml IL-4 (Peprotech). Cells from one femur and one tibia per animal (either male or female) were incubated in 10 ml of medium in a non-tissue culture coated 100 mm dish. Fresh GM-CSF and IL-4 were added to the media on a daily basis. At day 3, another 10 ml of fresh full medium containing 10 ng/ml GM-CSF and 10 ng/ml IL-4 was added to the culture dish. At day 6 and 8, half of the culture supernatant was collected, centrifuged, and the cell pellet resuspended in 10 ml fresh full medium containing 10 ng/ml GM-CSF and 10 ng/ml IL-4, and added back to the original plate. At day 8, DCs were ready for use in experiments.

Filipin Staining

BM derived DCs from DC-ABC^{DKO} and control mice were fixed in 4% paraformaldehyde. Cells were washed, and incubated in 1.5 mg glycine/ml to quench the paraformaldehyde. Cells were stained using 100 μg/mL filipin (Sigma) for 1 h at room temperature. After another wash, cells were mounted using Mowiol (Calbiochem) and visualized with an Axioskop 2 FS MOT upright confocal microscope (Zeiss). Images were obtained by implementing z-scanning and analyzed using Image J software. n=5 fields.

Flow Cytometry

Blood samples were collected by tail bleeding into EDTA coated tubes. For analysis of blood T-cells, tubes were kept at 4°C for the whole procedure unless stated otherwise. Red blood cells (RBCs) were lysed (BD Pharm Lyse, BD Bioscience) and white blood cells (WBCs) were centrifuged, washed, and resuspended in HBSS (0.1% BSA, 5 mM EDTA). Cells were stained with a cocktail of antibodies against CD45-APC-Cy7, Ly6-C/G-PerCP-Cy5.5 (BD Pharmingen), CD115-PE, CD44-PE-Cy7, CD62L-APC or CXCR3-APC, CD8-FITC (eBioscience), and TCRβ-PB (Biolegend). CD4^{+} T-cells were identified as CD45^{+}Ly6-C/G^{-}CD115^{-}TCRβ^{+}CD8^{-} and CD8^{+} T-cells as CD45^{+}Ly6-C/G^{-}CD115^{-}TCRβ^{+}CD8^{+}. Among these populations, activated T-cells were identified as CD44^{+}CD62L^{-} or CXCR3^{+}. The same stainings were carried out on LN and splenic homogenates, after incubation of axillary and inguinal LNs in collagenase D (clostridium histolyticum, Roche) for 30 min at 37°C or RBC lysis of spleens. LN and splenic homogenates were stained with the Mouse Regulatory T Cell Staining Kit (eBioscience) for analysis of T_{regs}. n=7-8 mice per genotype were used for each experiment. For analysis of DCs, splenic homogenates were stained with a cocktail of antibodies against F480-PE-Cy7, MHCII-FITC (eBioscience), CD11c-PerCP-Cy5.5 (BD Pharmingen), CD11b-APC, CD8-APC-Cy7, CD86-PE, PD-L1-PE (eBioscience) and CD80-PB (Biolegend), or the common β subunit for the IL-3/GM-CSF receptor (BD Pharmingen). For intracellular cytokine staining,

splenic homogenates were stained with CD11c-PE-Cy7, MHCII-FITC (BD Pharmingen), CD11b-APC or CD11b-PB (eBioscience), then fixed-permeabilized using the BD Cytofix/Cytoperm kit (BD Biosciences), and subsequently stained with pro-IL-1β-PE, p40-APC, or IL-6-PB, or their isotype controls (eBioscience). n=4-6 mice per genotype were used for each experiment.

To analyze neutral lipid accumulation in DCs, Bodipy-FITC (Thermo Fisher) was used. For analysis of spleen GM-CSF$^+$ T-cells, T-cell levels of T_{bet}, or T_h17-cells, spleen homogenates were first stained with TCRβ-PB (Biolegend), CD4-APC, CD8-FITC (eBioscience), or for CD4-PB (T_h17 cells; eBioscience) then fix-permeabilized, and subsequently stained with GM-CSF-PE, T_{bet}-PE, or IL17A-FITC, or their isotype controls (eBioscience). For analysis of T follicular helper cells, spleen homogenates were stained with TCRβ-PB (Biolegend), CD4-APC, CXCR5- PerCP-Cy5.5, and PD1-FITC (eBioscience). T follicular helper cells were defined as TCRβ$^+$CD4$^+$CXCR5$^+$PD1$^+$. For analysis of GC B-cells, spleen homogenates were stained with B220-FITC (Biolegend) and GL7-APC (eBioscience). GC B-cells were defined as B220$^+$GL7$^+$. For analysis of plasma cells, spleen homogenates were stained with CD19-PE (Biolegend) and CD138-APC (BD Pharmingen). Plasma cells were defined as CD19$^-$CD138$^+$. n=5-8 mice per genotype were used for these experiments. All samples were analyzed on an LSRII (BD Biosciences), running FACSDiVa software.

To assess *Abca1* and *Abcg1* mRNA expression in T-cells from T-ABC^{DKO} mice and their littermate controls, blood CD45$^+$CD115$^-$ Ly6-C/G$^-$TCRβ$^+$ cells were isolated using flow cytometry and sorted directly into RNeasy lysis buffer (Qiagen) using the FACSAria, running FACSDiVa software. The same procedure was followed to assess *Abca1* and *Abcg1* mRNA expression in CD45$^+$CD115$^-$ Ly6-C/G$^-$CD11c$^+$MHCII$^+$ splenic DCs, or to assess mRNA levels of *IL-23p19*, *GM-CSFRβ*, *pro-IL-1β,* and *Nlrp3* in CD45$^+$CD115$^-$ Ly6-C/G$^-$CD11c$^+$CD11b$^+$MHCII$^+$ splenic DCs. The cells were lysed in RNeasy lysis buffer, and RNA was then extracted using an RNeasy Micro Kit (Qiagen) and cDNA synthesized using SuperScript VILO (Invitrogen). mRNA levels were assessed using qPCR on a Stratagene Mx3000P (Agilent Technologies), and initial differences in RNA quantity were corrected for using the housekeeping gene m36B4. n=4-6 mice were used per genotype.

Microarray

Microarray analysis was carried out as part of the Immunological Genome Project (http://www.immgen.org), GSE#15907, as described (Gautier et al., 2012).

Antigen Presentation *In Vivo*

DC-ABC^{DKO} and control female mice were injected with or without 20 μg 332-339 ovalbumin peptide (OT-II peptide; Anaspec CA). At 24 h after injection, mice were injected with 2*10^6 cells 10 μM CFSE-PB labeled CD90.1$^+$CD4$^+$ OT-II T-cells. Briefly, CFSE-PB labeled CD4$^+$ OT-II cells were prepared by isolating CD4$^+$ T-cells from the spleen homogenates of CD90.1 OT-II female or male mice using CD4 coated magnetic beads (Miltenyi Biotec, CA) according to the manufacturer's instructions. CD90.1$^+$CD4$^+$ OT-II T-cells were labeled with 10 μM CFSE-PB (Life Technologies) according to the manufacturer's instructions. At 72 h after injection with the CD90.1$^+$CD4$^+$ OT-II T-cells, mice were sacrificed and LNs and spleens were isolated. Following homogenization over a 40 μm filter, LN and splenic T-cells were stained using CD4-APC, CD90.1-PE, and CD90.2-FITC (eBioscience), and CFSE-PB dilution was assessed using flow cytometry. All samples were analyzed on an LSRII (BD Biosciences), running FACSDiVa software. n=4 mice per genotype were used for this experiment.

Antigen Presentation *In Vitro*

BM derived DCs from DC-ABC^{DKO} and control mice were incubated with or without lipopolysaccharide (LPS) for a period of 24 h (250 ng/ml). Subsequently, cells were incubated with CD4$^+$OTII$^+$ T-cells that had been isolated as described above for *in vivo* antigen presentation, and were labeled with 5 μM CFSE-PB (Life Technologies) according to the manufacturer's instructions. At 72 h after incubation, T-cells were stained using CD4-FITC (eBioscience) and CFSE dilution was assessed using flow cytometry. All samples were analyzed on an LSRII (BD Biosciences), running FACSDiVa software. n=4 mice per genotype were used for this experiment.

Primary DC Isolation and Analysis, DC-T-Cell Co-incubation Experiments

CD11c$^+$ and CD11b$^+$ cells were isolated from LN and spleen homogenates using CD11b and CD11c coated magnetic beads (Miltenyi Biotec, CA) according to the manufacturer's instructions. Cells were cultured in 96 well plates in DMEM supplemented with 10% FBS and 1% pen-strep, and incubated with or without 20 ng/ml GM-CSF for 24 h (CD11c$^+$) or with and without 50 μg/ml rHDL (CSL-111, a kind gift from Dr. Samuel Wright, CSL Australia) (CD11b$^+$) for 24 h. Levels of IL-1β, IL-18, IL-23, IL-12p70, and IL-6 were measured in the media using ELISA (R&D systems), and corrected for cell protein. For Western blot to assess caspase-1 cleavage in CD11b$^+$ cells, a primary rat anti-mouse caspase-1 antibody (eBioscience) and a rat secondary antibody (Cell-Signaling) were used. For co-incubation experiments, CD11c$^+$ DCs were incubated with T-cells isolated from 8 week old wild-type mice using CD3ε$^+$ beads (Miltenyi Biotec) in a ratio 1:5 for 5 days. T_h17 and GM-CSF$^+$ T-cells were assessed as described above in 'flow cytometry'. For each experiment, one replicate of CD11c+ or CD11b+ DCs represented one mouse. n=4 mice per genotype were used for each experiment.

QUANTIFICATION AND STATISTICAL ANALYSIS

All data are presented as means ± SEM. In each experiment, n defines the number of mice included, except for the filipin staining experiment, where n represents the number of fields. The statistical parameters (n, mean, SEM) can be found within the figure legends. The t-test was used to define differences between 2 datasets. To define differences between 3 or 4 datasets, One-way Analysis

of Variance (ANOVA) was used with a Bonferroni multiple comparison post-test. The criterion for significance was set at $P<0.05$. No statistical method was used to determine whether the data met assumptions of the statistical approach. Statistical analyses were performed using GraphPad Prism version 5.01 (San Diego, CA).

DATA AND SOFTWARE AVAILABILITY

The accession number for the microarray data reported in this paper is: http://www.immgen.org : GSE#15907, as described (Gautier et al., 2012).

Cell Metabolism, Volume *25*

Supplemental Information

Cholesterol Accumulation in Dendritic Cells Links the Inflammasome to Acquired Immunity

Marit Westerterp, Emmanuel L. Gautier, Anjali Ganda, Matthew M. Molusky, Wei Wang, Panagiotis Fotakis, Nan Wang, Gwendalyn J. Randolph, Vivette D. D'Agati, Laurent Yvan-Charvet, and Alan R. Tall

Supplemental Figures

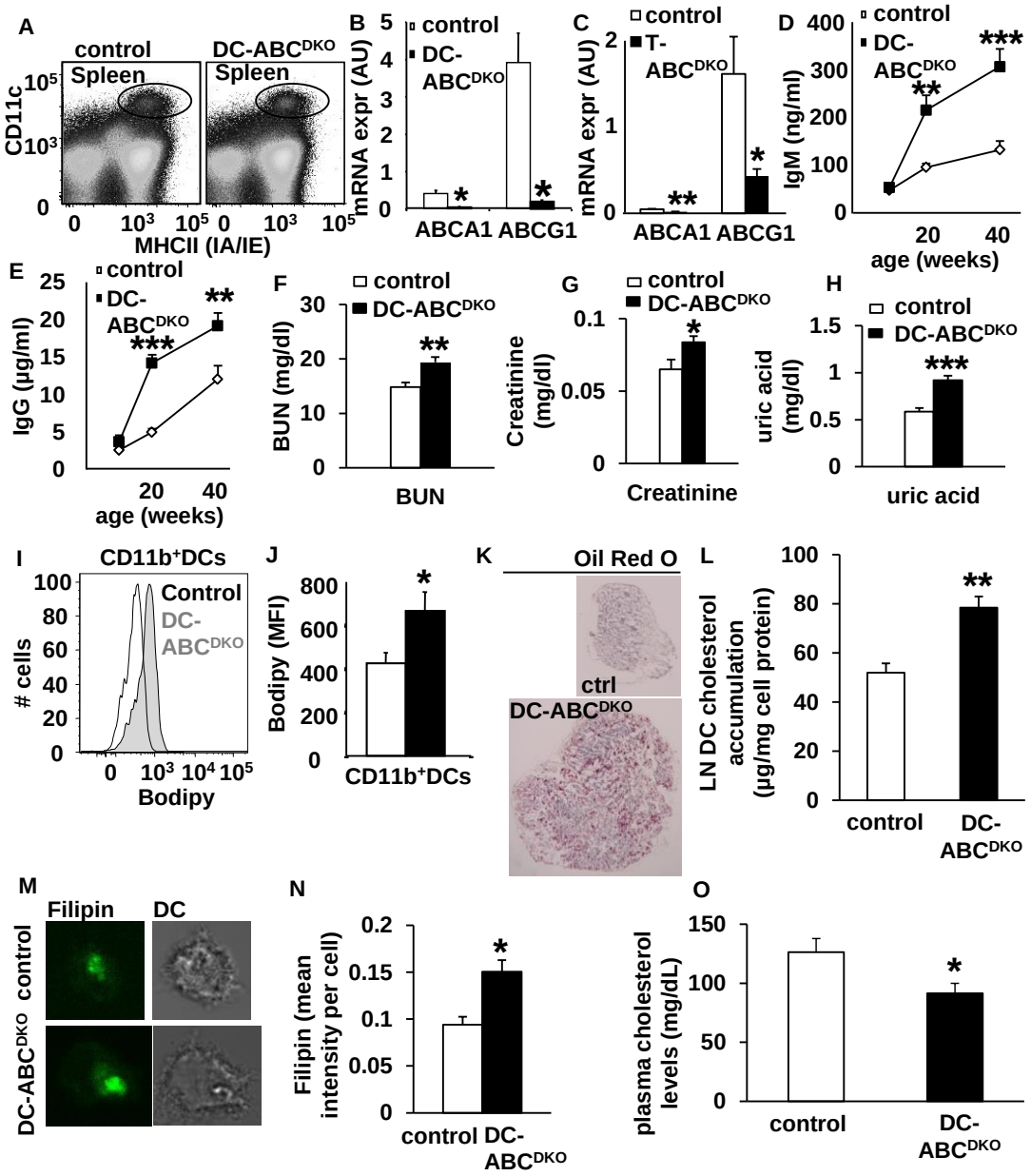

Figure S1, related to Figure 2. DC-ABC^{DKO} and T-ABC^{DKO} mice show >90% and >80% decreased ABCA1 and ABCG1 mRNA expression in dendritic cells (DCs) and T-cells, respectively and DC-*Abca1/g1* deficiency induces lipid accumulation in DCs. (**A**) Gating strategy for isolation of splenic CD45^{+}CD115^{-}CD11c^{+}MHCII^{+} DCs in control and DC-ABC^{DKO} mice. (**B**) Splenic DCs were sorted by flow cytometry and the *Abca1* and *Abcg1* mRNA expression levels were determined and corrected for the housekeeping gene m36B4. n=6. (**C**)

Blood $CD4^+$ T-cells were sorted by flow cytometry and the *Abca1* and *Abcg1* mRNA expression levels were determined and corrected for the housekeeping gene m36B4. n=4. (**D-E**) Increased plasma levels of IgM (**D**) and IgG (**E**) in DC-ABC^{DKO} mice. n=6-10. (**F-H**) Increased plasma levels of blood urea nitrogen (BUN) (**F**), creatinine (**G**), and uric acid (**H**) in DC-ABC^{DKO} mice. n=10. (**I-J**) Increased lipid accumulation in splenic DC-ABCDKO $CD11b^+$ DCs assessed by BODIPY staining. n=6. (**K**) Inguinal LNs were embedded in OCT and frozen sections were made and stained for Oil Red O. Lipid accumulation in DC-ABC^{DKO}, but not in control LNs. All sections (n=6) studied showed Oil Red O staining in DC-ABC^{DKO} but not in control LNs. Representative pictures are shown. (**L**) DC-*Abca1/g1* deficiency enhances cholesterol accumulation in DCs. $CD11c^+$ cells were isolated from the lymph nodes of control and DC-ABC^{DKO} mice using CD11c positive beads, lipids were extracted, and cholesterol was assessed using an enzymatic assay and corrected for cell protein. n=6. (**M-N**) Bone marrow cells were differentiated into DCs by treatment with GM-CSF and were stained with filipin. Representative pictures of n=5 fields are shown (**M**) and filipin staining was quantified (**N**). (**O**) Plasma cholesterol levels in 20 week old control and DC-ABC^{DKO} mice fed a chow diet. n=10. Data in **B**, **C-H**, **J**, **L**, **N**, and **O** are presented as mean ± SEM. **P*<0.05, ***P*<0.01, ****P*<0.001, by t-test.

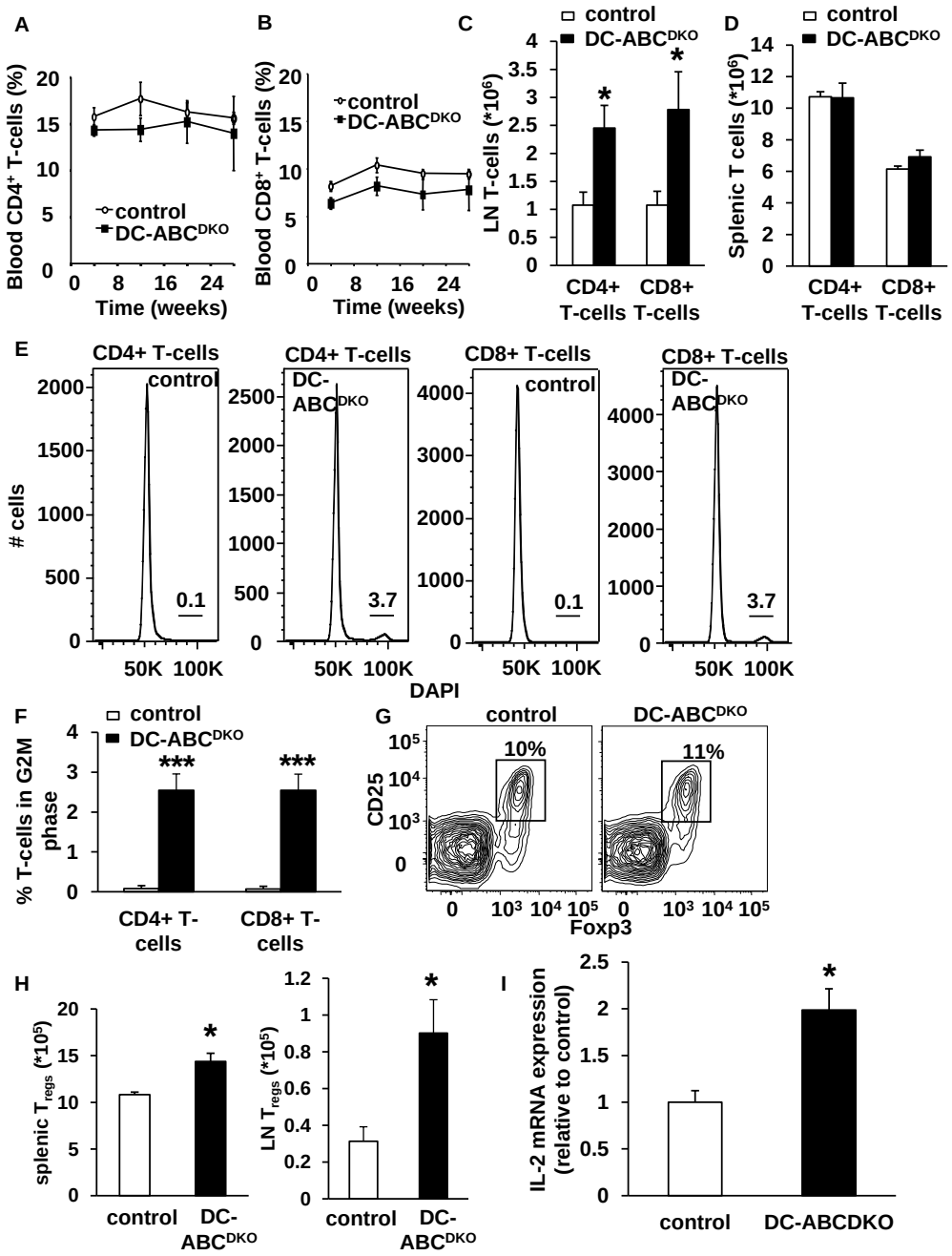

Figure S2, related to Figure 3. Effect of DC *Abca1/g1* deficiency on CD4$^+$ and CD8$^+$ T-cell numbers, T-cell proliferation, and T_{regs}. CD4$^+$ and CD8$^+$ T-cell percentage was assessed in blood (**A**-**B**), and CD4$^+$ and CD8$^+$ T-cell numbers in inguinal lymph nodes (**C**) and spleen (**D**) n=5-8. All data in (**A**-**D**) were measured concurrently with T-cell activation measurements. (**E** and **F**) CD4$^+$ and CD8$^+$ T-cell proliferation was assessed using DAPI in lymph nodes and

calculated in Flow Jo using the Watson model. (**E**) T-cell proliferation graphs. Percentages show cells in the G2M phase. (**F**) Quantification of T-cells in the G2M phase. n=5. (**G**) and (**H**) DC-ABC^{DKO} mice show increased T_{regs} in spleen and lymph nodes. (**G**) Gating strategy. (**H**) Splenic T_{reg} and lymph node T_{reg} numbers. n=7. (**I**) DC-ABC^{DKO} increases IL-2 mRNA in CD4^{+} T-cells. CD4^{+} T-cells were sorted from LNs using flow cytometry, RNA extracted, and IL-2 mRNA levels assessed. Data in **A-D**, **F**, **H**, and **I** are presented as mean ± SEM. **P*<0.05, ****P*<0.001, by t-test.

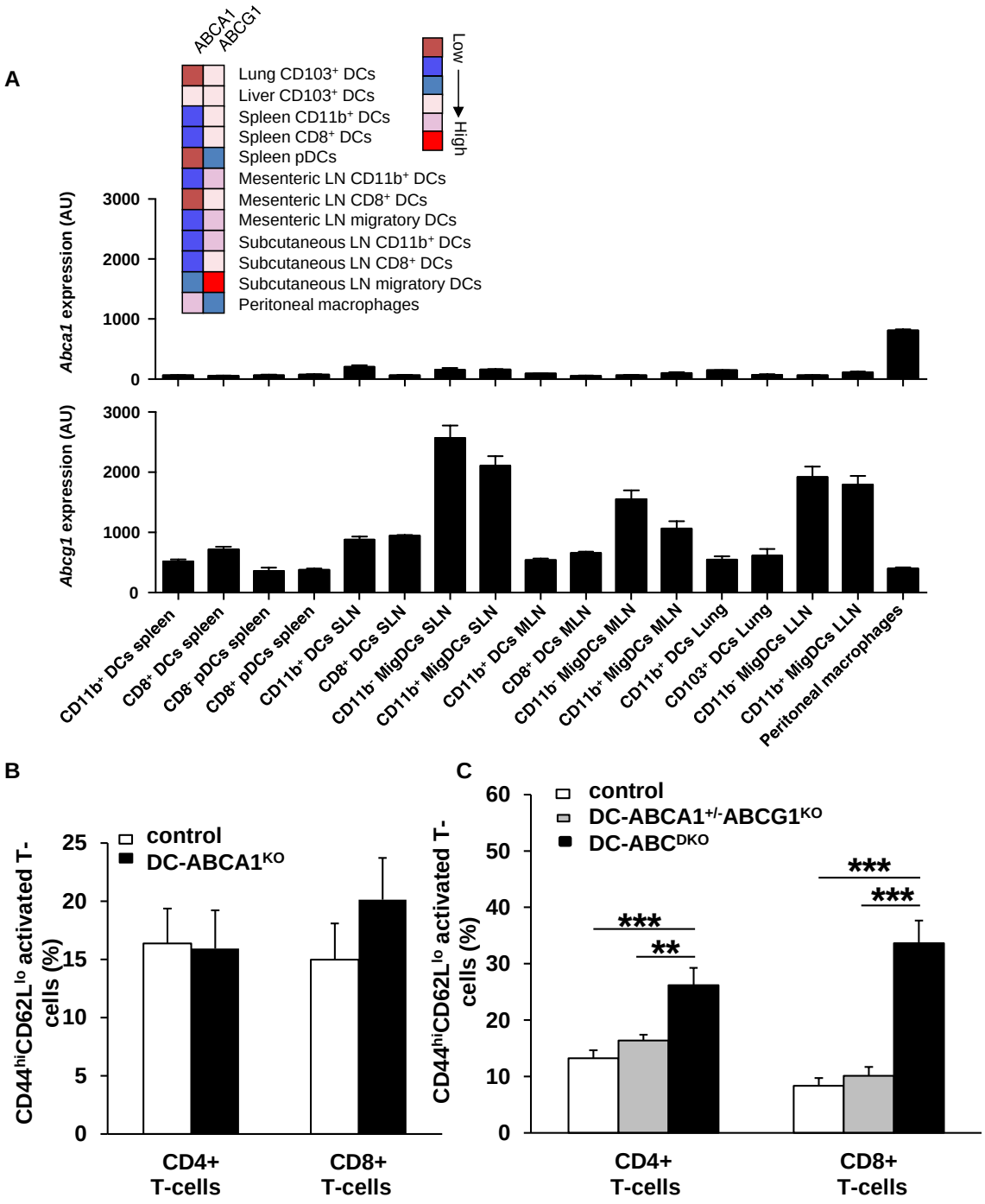

Figure S3, related to Figure 3. ABCG1 is highly expressed in several DC subtypes but only combined deficiency of ABCA1 and ABCG1 induces T-cell activation. (**A**) Expression of *Abca1* and *Abcg1* in several DC subtypes and peritoneal macrophages as assessed by microarray. Top: heatmap. Bottom: quantification of *Abca1* and *Abcg1* expression. These data were obtained

as part of the Immunological Genome Project. (**B-C**) Combined deficiency of ABCA1 and ABCG1 in DCs is required for the T-cell activation phenotype. (**B**) $CD44^{hi}CD62L^{lo}$ activated $CD4^{+}$ and $CD8^{+}$ T-cells in the blood of control and DC-$ABCA1^{KO}$ mice. n=5. (**C**) $CD44^{hi}CD62L^{lo}$ activated $CD4^{+}$ and $CD8^{+}$ T-cells in the blood of control, DC-$ABCA1^{+/-}$ $ABCG1^{KO}$ and DC-ABC^{DKO} mice. n=5. **B** and **C**, $^{**}P<0.01$, $^{***}P<0.001$, by one-way ANOVA with Bonferroni post-test.

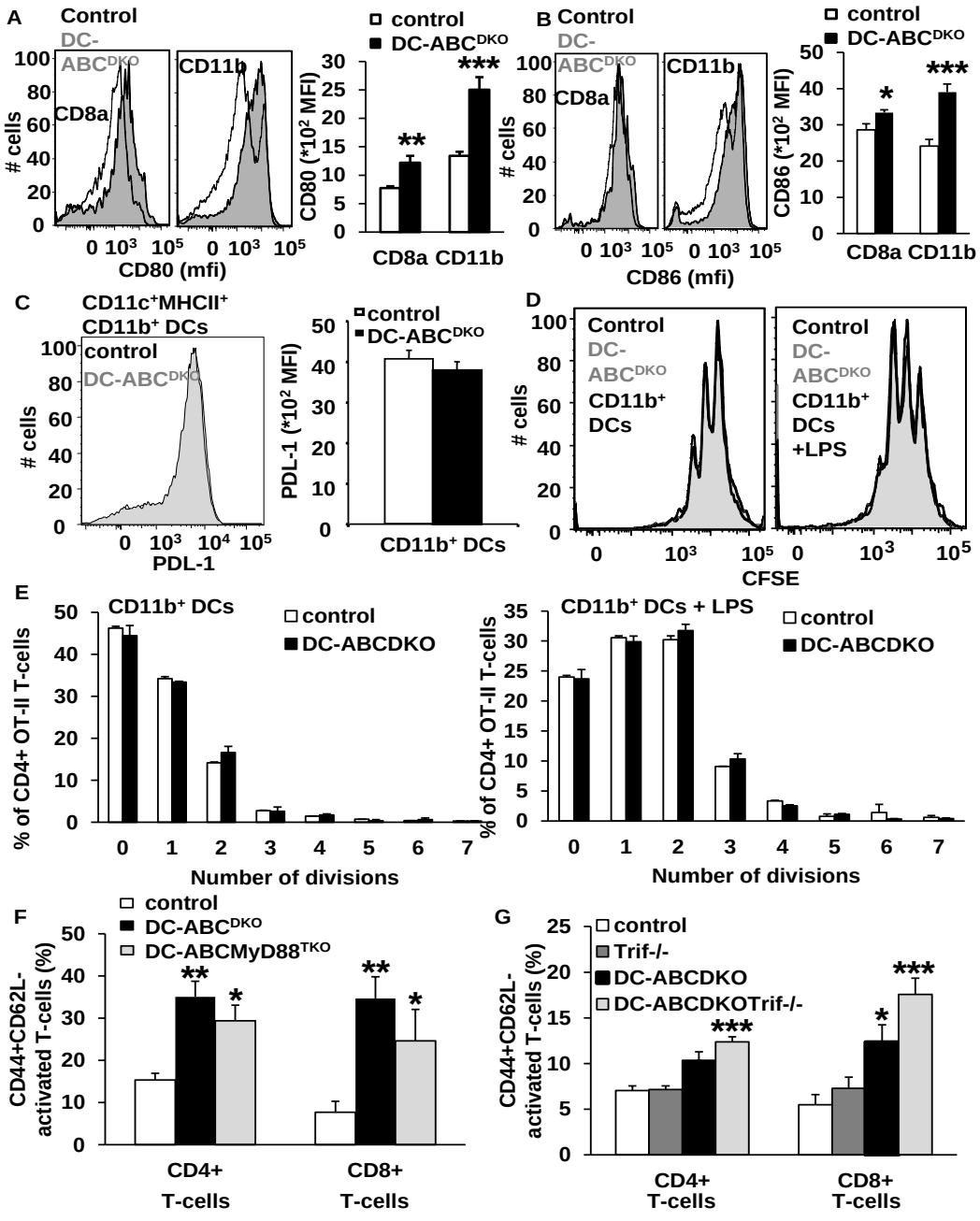

Figure S4, related to Figure 4. DC-*Abca1/g1* deficiency enhances CD80/86 expression, but does not affect PDL-1 surface expression in CD11b^{+} DCs and antigen presentation by CD11b^{+} DCs *in vitro*, and T-cell activation in DC-ABC^{DKO} mice is not due to enhanced MyD88 or Trif signaling. (**A-C**) CD80 (**A**) and CD86 (**B**) surface levels on splenic CD11c^{+}MHC-II^{+}CD8a^{+} and CD11c^{+}MHC-II^{+}CD11b^{+} DCs and PDL-1 (**C**) surface levels on

splenic $CD11c^+MHC\text{-}II^+CD11b^+$ DCs determined by flow cytometry. Representative examples and quantification. n=4-6. *P<0.05, **P<0.01, ***P<0.001, by t-test. (**D**-**E**) Bone marrow cells were stimulated with GM-CSF for 8 days to generate $CD11b^+$ DCs, incubated with or without LPS for 24 h, and then incubated with OT-II peptide in the presence of CFSE labeled $CD4^+$OTII T-cells (ratio DC:T-cells 1:5). CFSE dilution in $CD4^+$ T-cells was assessed at 72 h after co-incubation. Representative CFSE dilutions are shown (**D**) and quantified using Flow Jo software (**E**). n=4. Mice were fed chow diet for 16-20 weeks (**F** and **G**) and activated $CD44^+CD62L^-$ $CD4^+$ and $CD44^+CD62L^-$ $CD8^+$ T-cells in blood were measured using flow cytometry. n=6. The experiment was done twice at different timepoints. Data are presented as mean ± SEM. *P<0.05, **P<0.01, ***P<0.001, compared to control, by one way ANOVA and Bonferroni post-test.

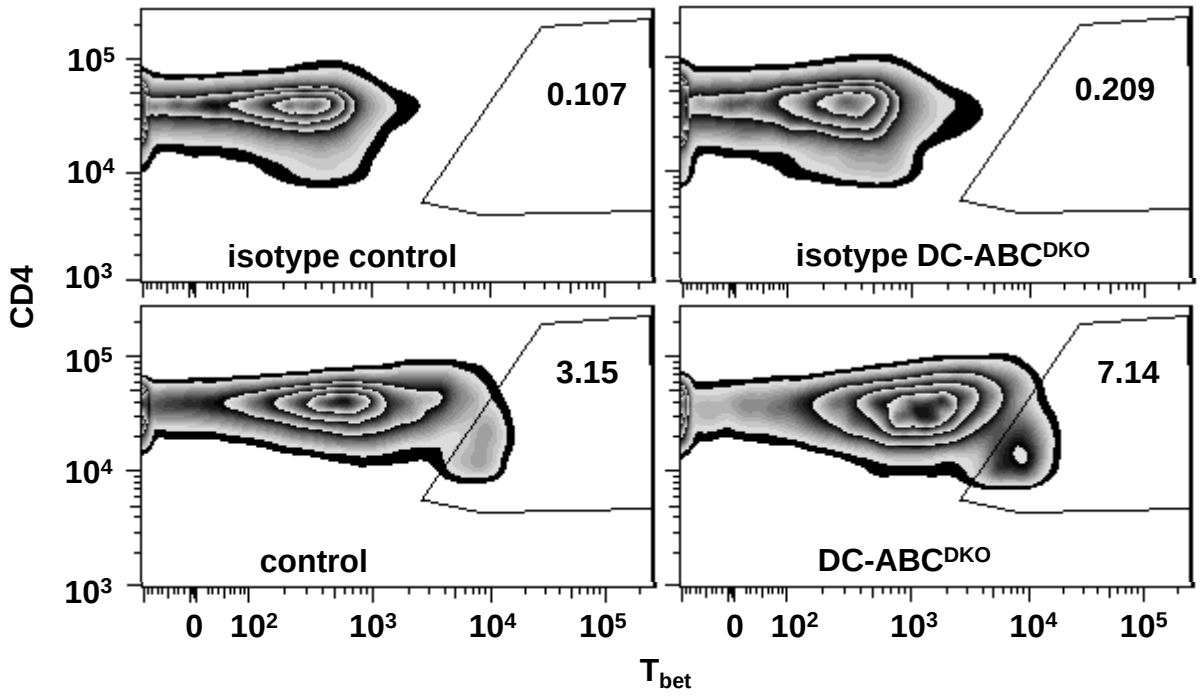

Figure S5, related to Figure 5. Splenic cell homogenates were stained with an antibody to CD4, fixed and permeabilized, and stained for T_{bet} or its isotype control. Representative FACS plots are shown.

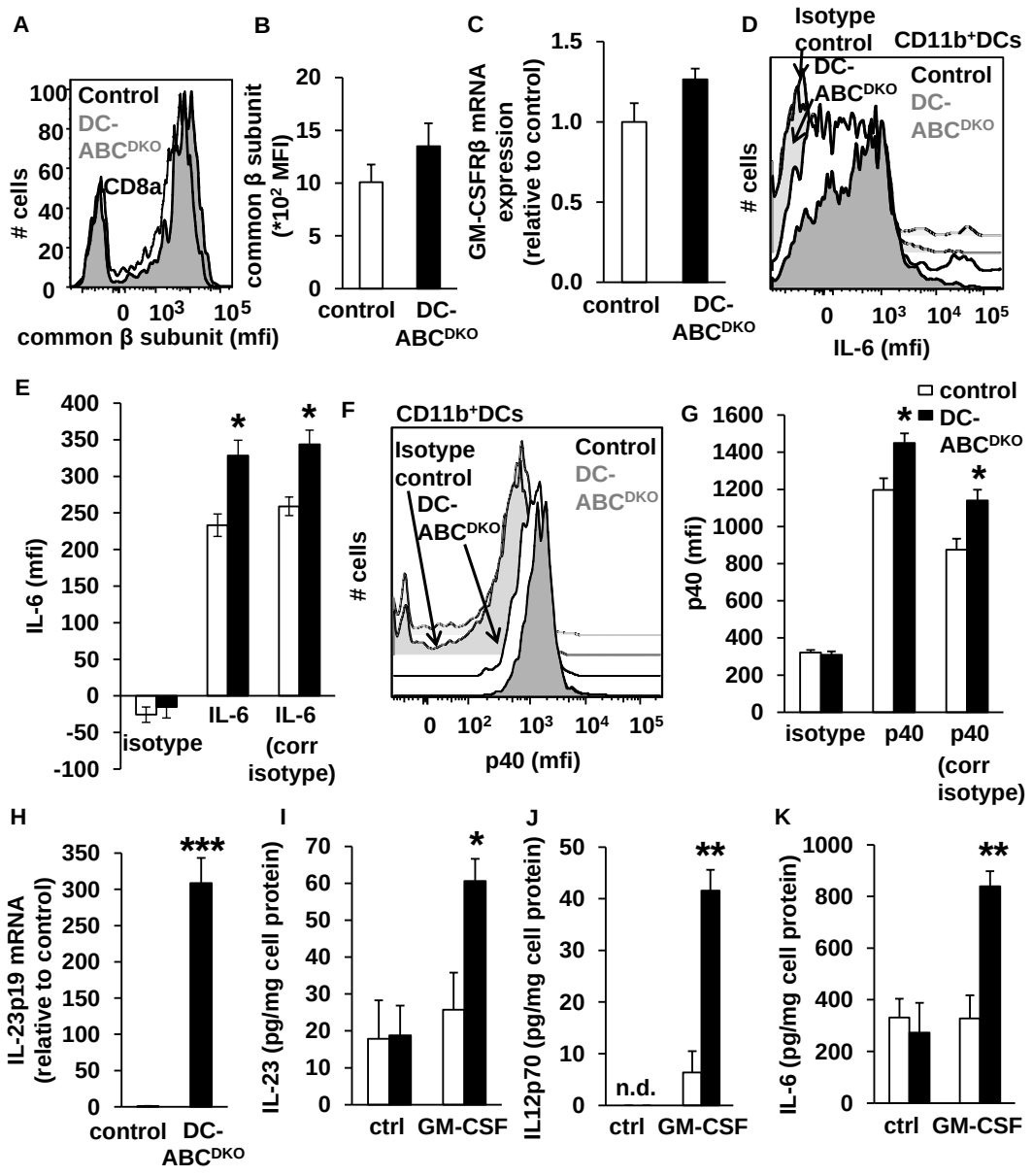

Figure S6 related to Figure 7. DC *Abca1/g1* deficiency does not affect GM-CSFRβ surface on CD8a$^+$ DCs or GM-CSFRβ mRNA expression in CD11b$^+$ DCs, but enhances intracellular cytokines in CD11b$^+$ DCs, and secretion of interleukins induced by GM-CSF in CD11c$^+$ DCs. Spleens were isolated from 20 week old mice. Spleens were isolated (**A-B**), stained for DC markers in combination with the indicated antibodies, and analyzed by flow cytometry. (**A-B**) DC-*Abca1/g1* deficiency did not affect the surface level of the common β subunit of the GM-CSF receptor on splenic CD8a$^+$ DCs. n=6. (**C**) CD11c$^+$MHCII$^+$CD11b$^+$ DCs were sorted using flow cytometry, RNA was extracted and GM-CSFRβ mRNA levels assessed. n=4. (**D-G**) Intracellular staining of IL-6 (**D**, **E**), and p40 (**F**, **G**) in CD11c$^+$MHCII$^+$CD11b$^+$ DCs.

FACS plots (**D**, **F**) and quantifications (**E**, **G**) are shown. n=4. (**H**) IL23p19 mRNA levels in $CD11c^{+}MHCII^{+}CD11b^{+}$ DCs as sorted in (**C**). n=4. (**I-K**) $CD11c^{+}$ cells were sorted from the spleen of 20 week old control and $DC\text{-}ABC^{DKO}$ mice using CD11c positive beads and then incubated with or without GM-CSF (20 ng/ml) for 24 h. IL-23 (**I**), IL-12p70 (**J**), and IL-6 (**K**) secretion were assessed and corrected for cell protein. n=4. Data in **B**, **C**, **E**, **G-K** are presented as mean ± SEM. **P*<0.05, ***P*<0.01, ****P*<0.001, by t-test.

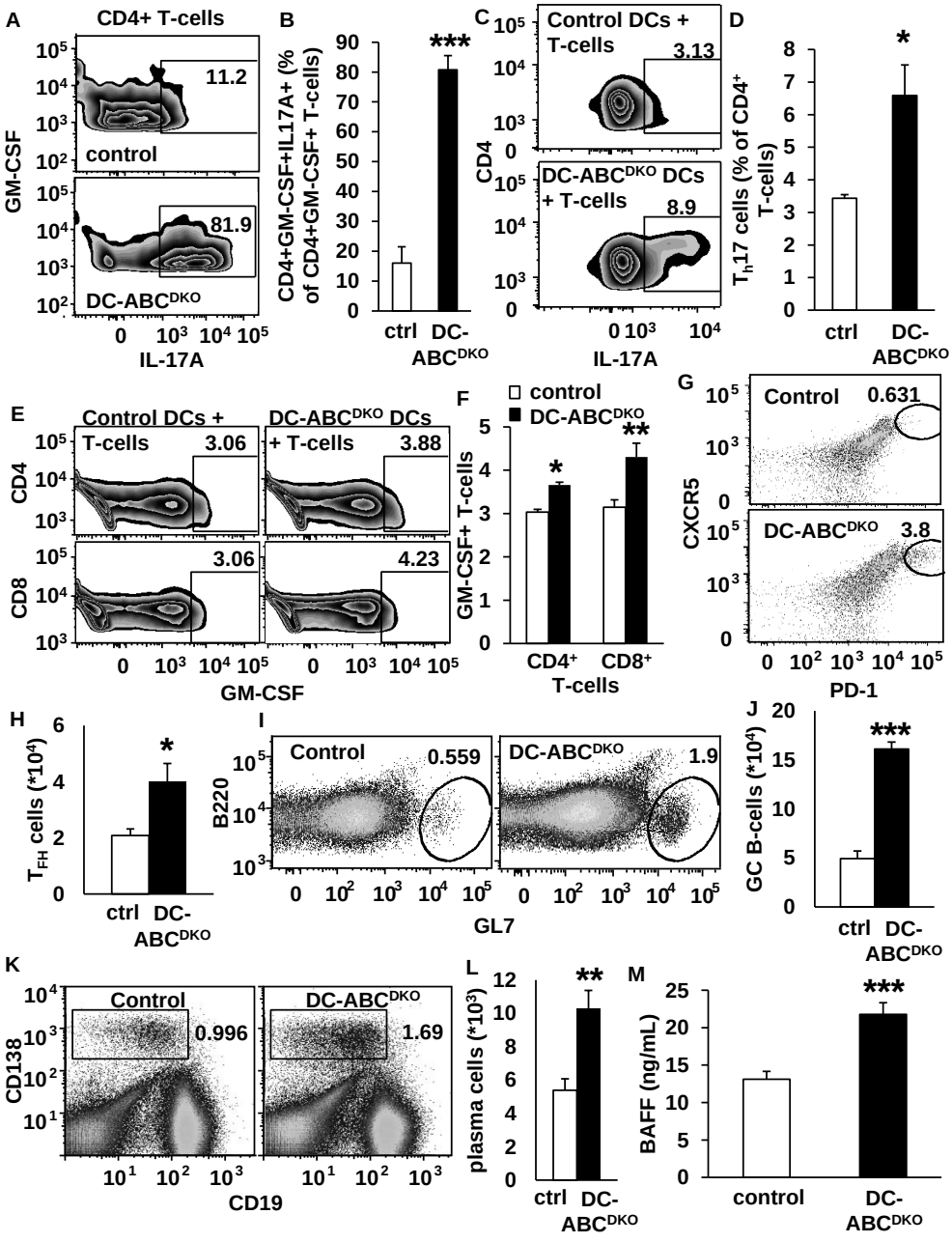

Figure S7, related to Figure 7. DC-*Abca1/g1* deficiency leads to expansion of several T-cell subsets. Spleens were isolated from 20 week old mice. (**A-B**) In DC-ABC^{DKO} mice, GM-CSF^{+} T-cells are highly positive for IL17A. Splenic cell homogenates were stained with antibodies to CD4, fixed and permeabilized, stained for GM-CSF and IL17A, and IL17A expression was

assessed in GM-CSF$^+$ T-cells. FACS plots (**A**), and quantification (**B**). n=4. (**C-F**) *Abca1/g1* deficiency in DCs stimulates differentiation of T-cells towards T_h17 cells (**C-D**) and GM-CSF$^+$ T-cells (**E-F**) in co-incubation experiments of DCs with naïve T-cells. CD11b$^+$ DCs were isolated from splenic homogenates of control and DC-ABC^{DKO} mice using CD11b$^+$ beads and co-incubated with splenic T-cells of 8 week old wild-type mice. Cells were co-cultured in a DC:T-cell ratio of 1:5 for 5 days and subsequently stained with antibodies to CD4, fixed and permeabilized, stained for IL17A, and T_h17-cells were assessed (**C-D**). n=4. Alternatively, after co-incubation, cells were stained with antibodies to CD4 and CD8, fixed and permeabilized, stained for GM-CSF and GM-CSF$^+$ T-cells were assessed (**E-F**). n=4. (**G-L**) Splenic T- and B-cell subsets were analyzed by flow cytometry. T follicular helper (T_{FH}) cells were identified as TCRβ$^+$CD4$^+$CXCR5$^+$PD1$^+$ (**G-H**). Germinal center B-cells were identified as B220$^+$GL7$^+$ (**I-J**). Plasma cells were identified as CD19$^-$CD138$^+$ (**K-L**). n=6. (**M**) DC-*Abca1/g1* deficiency increased plasma BAFF levels. n=10. Data in **B**, **D**, **F**, **H,** **J**, **L**, and **M** are presented as mean ± SEM. **P*<0.05, ***P*<0.01, ****P*<0.001, by t-test.